Molecular Bases of Disease:

Molecular Interaction between the Chaperone Hsc70 and the N-terminal Flank of Huntingtin Exon 1 Modulates Aggregation

Elodie Monsellier, Virginie Redeker, Gemma Ruiz-Arlandis, Luc Bousset and Ronald Melki

J. Biol. Chem. published online December 10, 2014

Access the most updated version of this article at doi: 10.1074/jbc.M114.603332

JBC Papers in Press. Published on December 10, 2014 as Manuscript M114.603332
The latest version is at http://www.jbc.org/cgi/doi/10.1074/jbc.M114.603332

Molecular interaction between the chaperone Hsc70 and the N-terminal flank of Huntingtin Exon 1 modulates aggregation

Elodie Monsellier*, Virginie Redeker, Gemma Ruiz-Arlandis, Luc Bousset, and Ronald Melki*#

From the Laboratoire d'Enzymologie et Biochimie Structurales, CNRS, 91198 Gif-sur-Yvette, France

Running title: *Molecular interaction between Hsc70 and huntingtin exon1*

* To whom correspondence should be addressed: Elodie Monsellier, +33-16982-3486, monsellier@lebs.cnrs-gif.fr - Ronald Melki, +33-16982-3503, melki@lebs.cnrs-gif.fr

Keywords: heat shock protein (HSP); mass spectrometry (MS); molecular chaperone; neurodegenerative disease (ND); Huntington's disease (HD); polyglutamine; protein aggregation

Background: Hsc70 has an alleviating effect on the toxicity of polyglutamine (polyQ[1]) containing proteins *in vivo*
Results: Hsc70 binds specifically the N-terminal flank of huntingtin exon 1
Conclusion: Hsc70 interaction with huntingtin exon 1 N-terminal flank affects the conformation of the resulting assemblies
Significance: We identify the surface interfaces between Hsc70 and huntingtin exon 1 which allows the design of future therapeutic tools

ABSTRACT

The aggregation of polyglutamine (polyQ) containing proteins is at the origin of nine neurodegenerative diseases. Molecular chaperones prevent the aggregation of polyQ containing proteins. The exact mechanism by which they interact with polyQ containing, aggregation prone proteins and interfere with their assembly is unknown. Here we dissect the mechanism of interaction between huntingtin exon 1 fragment of increasing polyQ lengths (HttEx1Qn), which aggregation is tightly associated to Huntington's disease, with the molecular chaperone Hsc70. We show that Hsc70 together with its Hsp40 co-chaperones inhibit HttEx1Qn aggregation and modify the structural, seeding and infectious properties of the resulting fibrils in a polyQ-independent manner. We demonstrate that Hsc70 binds the 17-residues long N-terminal flank of HttEx1Qn and we map Hsc70-HttEx1Qn surface interfaces at the residue-level. Finally we show that this interaction competes with homotypic interactions between the N-termini of different HttEx1Qn molecules that trigger the aggregation process. Our results lay the foundations of future therapeutic strategies targeting huntingtin aggregation in Huntington's disease.

Huntington's diseases (HD) is a dominant heritable neurodegenerative disease tightly associated to the aggregation of the protein

We thank Nils Maréchal, Laetitia Thomas and Charlène Lasgi for experimental assistance. This work benefited from the IMAGIF and Institut Curie imaging and sorting facilities and the Mass Spectrometry facility of the Centre de Recherche de Gif and Federative Research Institute Genomes, Transcriptomes, Proteomes. This work was supported by the Agence Nationale de la Recherche (ANR-11-BSV8-021-01), the Centre National de la Recherche Scientifique, the Human Frontier Science Program, the European Community's Seventh Framework Program FP7/2010, Marie Curie Actions grant n° 264508, and a "Coup d'Elan à la Recherche Française" award from Fondation Bettencourt-Schueller.

[1] The abbreviations used are: polyQ, polyglutamine; Hsc, constitutive heat-shock protein; Htt, huntingtin; HttEx1Qn, huntingtin exon1 with a polyQ length of n; HD, Huntington's disease; Nt_{17}, 17-residue long N-terminal flank of HttEx1Qn; BS3, bis(sulfosuccinimidyl) suberate; ChFP, mCherry fluorescent protein.

huntingtin (Htt), a large protein of ~3144 residues generated through the expression of the 67 exons of the HTT gene, or a proteolytic N-terminal fragment of Htt corresponding to exon 1 (HttEx1Qn) (1–3). Htt plays critical roles in early development, in the regulation of gene transcription, in neurogenesis and cell survival and in axonal transport (4). The aggregation of Htt and HttEx1Qn occurs in individuals bearing an abnormally long homopolymeric tract of glutamine residues (polyQ) in the N-terminal part of Htt above a threshold of ~ 35Q due to the expansion of CAG tracts within the protein-coding region of the HTT gene (5, 6). HttEx1Qn with the expanded polyQ tract (n>35) aggregates in animal models for HD and *in vitro* into insoluble ß-sheet rich fibrillar assemblies (7, 8) that have prion-like properties (9, 10).

Synthetic and recombinant peptides made of 35 glutamines and over assemble in a nucleation dependent manner into fibrils resembling those HttEx1Qn with similar polyQ lengths form (11). However, as the polyQ stretch is flanked N- and C-terminally by 17 and 52 amino acid residues, respectively, with the C-terminal flank comprising two stretches of 11 and 10 proline residues separated by a 17 amino acid stretch mostly made of Q and P residues, studies aimed at documenting the way the polyQ context within HttEx1Qn, e.g. HttEx1Qn flanks, affects aggregation have been performed. While the C-terminal P-rich polyQ flank has been repeatedly shown to affect negatively aggregation (12), two models have been proposed to account for the role of the polyQ 17-residue long N-terminal flank (Nt_{17}) to HttEx1Qn aggregation (13, 14).

Molecular chaperones combat protein aggregation within the cells. The role of various molecular chaperones in polyQ-containing protein aggregation has been subject to active investigations, but their mode of action remain elusive. Various and sometimes contradictory effects have been reported in cellular or animal models (15–19). In addition, the existence of a direct interaction between the chaperones and the polyQ stretch *per se* is subject to debate (19–22) since the interaction between the chaperones and the hydrophilic polyQ stretch is *a priori* unfavorable (23, 24).

Here we assess the role and mechanism of action of the constitutively expressed heat shock protein Hsc70 and its co-chaperones from the Hsp40 family in HttEx1Qn aggregation. We show that Hsc70, in its active, functional form, affects HttEx1Qn assembly by interacting with the N-terminal flank of HttEx1Qn (Nt_{17}) in a manner independent from the polyQ stretch. We show that the fibrillar scaffold and *in vivo* seeding properties of HttEx1Qn fibrils assembled in the presence of Hsc70 are distinct from those of HttEx1Qn fibrils assembled in the absence of Hsc70. Using chemical cross-linking with the homobifunctional NHS-ester BS3, we bring evidence for an Hsc70-HttEx1Qn complex. We map the surface interface between Hsc70 and HttEx1Qn after identification of the cross-linked polypeptides by mass spectrometry analyses.

Our results highlight the importance of HttEx1 N-terminal flank in the assembly process of HttEx1Qn. Using the same cross-linking strategy as above, we demonstrate Nt_{17}-Nt_{17} interaction in the early stages of HttEx1Qn coalescence during assembly into fibrils. Identification of the cross-linked polypeptides, together with the fact that Nt_{17} is α-helical lead us to propose a model for on-assembly pathway oligomeric HttEx1Qn species that integrates structural constraints.

EXPERIMENTAL PROCEDURES

Expression and purification of recombinant polypeptides and synthetic Nt_{17} peptides. Recombinant C-terminally hexa His-tagged MBP-TEV-HttEx1Qn-His with various polyQ lengths (n = 17, 25, 30, 35, 41 or 48) was expressed in *E. coli* strain BL21(DE3) (Stratagene, Santa Clara, CA, USA), and purified in two steps. The protein lysate was first loaded on a 10 ml bed volume amylose resin column (New England Biolabs) equilibrated in 20 mM Tris-HCl pH 7.5, 150 mM KCl, 10% glycerol, 1 mM 2-β-mercaptoethanol. The MBP-TEV-HttEx1Qn-His was eluted from this column with 10 mM maltose and its concentration was determined from its absorbance at 280 nm using an extinction coefficient of 67840 M^{-1} cm^{-1} for all the polyQ lengths. MBP-TEV Protease, produced using the plasmid pRK1043 (Addgene, Cambridge, MA, USA), was added to the eluted protein at 1:5 ratio (w/w) and 100% cleavage, as assessed using SDS-PAGE, was achieved upon

incubating the mixture for 1 h at 37°C. The mixture was loaded on a 5 ml bed volume Talon metal affinity resin column (Clontech, Saint-Germain-en-Laye, France), the column was washed with 20 bed volumes of either 20 mM Tris-HCl, pH 7.5, 150 mM KCl, 10 mM imidazole and 10% glycerol or 40 mM Hepes-OH, pH 7.5, 75 mM KCl, 10 mM imidazole and 10% glycerol for cross-linking experiments, and HttEx1Qn-His (**Fig. 1A**) eluted in the same buffer complemented with 200 mM imidazole. The protein was immediately filtered through a 0.22 μM filter, aliquoted, flash frozen in liquid nitrogen and stored at -80°C until use. The temperature, protein concentration and buffer conditions were optimized so that the cleaved HttEx1Qn would remain soluble during the whole purification process. HttEx1Qn concentration was determined by SDS-PAGE quantification following Sypro staining and integration using a LAS-3000 imager (Fujifilm, Tokyo, Japan) and the software Multigauge (Life Science Systems). Qn and HttEx1Qn-ΔNt_{17} (**Fig. 1A**) were obtained following the same procedure.

Recombinant hexa His-tagged wildtype Hsc70, Hdj1 and Hdj2 were purified as previously described (25). Concentrations were determined spectrophotometrically using the following extinction coefficients at 280 nm: 39310 $M^{-1}cm^{-1}$ for Hsc 70, 9970 $M^{-1}cm^{-1}$ for Hdj1, and 16390 $M^{-1}cm^{-1}$ for Hdj2. Pure Hsc70, Hdj1 and Hdj2 in 50 mM Tris-HCl, pH 7.5, 150 mM KCl, 5 mM β-mercaptoethanol, 5 mM $MgCl_2$, 1 mM EGTA and 10% glycerol were aliquoted and stored at -80°C. Hsc70 was also stored in 40 mM Hepes-OH, pH 7.5, 75 mM KCl, 5 mM β-mercaptoethanol, 5 mM $MgCl_2$, 1 mM EGTA and 10% glycerol. To make sure that Hsc70 and its co-chaperones are functional, their luciferase refolding activities and their ATPase activities were monitored as described (25).

The peptides Nt_{17} (MATLEKLMKAFESLKSF), dansyl-Nt_{17} (**Fig. 1A**) and its scrambled form (dansyl-MLTFAEFKSMELKSLAK) were purchased from GL Biochem Ltd (Shangaï). Peptides were dissolved in HFIP, aliquoted, and stored after evaporation of HFIP under N_2 at -20°C. All peptides were resuspended in DMF at a final concentration of 2 mM.

Assembly of HttEx1Qn, Qn or HttEx1Qn-ΔNt_{17} into fibrils and monitoring of the aggregation reactions. Soluble HttEx1Qn, Qn or HttEx1Qn-ΔNt_{17} were assembled in 20 mM Tris-HCl, pH 7.5, 150 mM KCl, 5 mM $MgCl_2$, 1 mM ATP, 100 mM imidazole and 10% glycerol, with or without Hsc70, Hdj1, Hdj2 or Nt_{17}, alone or in combination, at 37°C without shaking. For thioflavin T measurements, aliquots (100 μL) were withdrawn and immediately mixed with thioflavin T (10 μM final). The fluorescence was measured on a Cary Eclipse Fluorescence Spectrophotometer (Varian Medical Systems Inc., California, USA) using the following settings: excitation wavelength = 440 nm; emission wavelength = 480 nm; excitation and emission slits = 5 and 10 nm, respectively.

For SDS-PAGE analyses, aliquots (8 μL) were removed at different time intervals, immediately mixed with denaturing buffer (180 mM Tris-HCl pH 6.8, 30% glycerol, 15% β-mercaptoethanol, 6% SDS), incubated for exactly 5 min at 95°C and frozen at -70°C until analysis on 12-15% Glycine- SDS-PAGE. The gels were washed in water, stained by SYPRO Orange (Invitrogen, Paisley, UK) diluted 5000 fold in acetic acid 10% for 1h and visualized using a LAS-3000 imager (Fujifilm, Tokyo, Japan). The amount of SDS-soluble and SDS-insoluble species trapped in the stacking gel was quantified using the software Multigauge (Life Science Systems). For each time point t the fraction f_t of assembled polypeptides was extrapolated from these values and plotted versus time. The plots were fitted to the following empirical sigmoid function:

$$f_t = f_\infty / \{1 + \exp[k_{elong} \bullet (t_{1/2} - t)]\}$$

where f_∞ is the fraction of assembled polypeptide at the end of the reaction, k_{elong} is the elongation slope, and $t_{1/2}$ is the aggregation half-time. The lag phase duration t_{lag} was determined from k_{elong} and $t_{1/2}$ as follows:

$$t_{lag} = t_{1/2} - \ln(2/k_{elong})$$

For each protein variant we recorded at least three independent kinetics of aggregation. The presence of fibrillar material at the end of the aggregation process was systematically assessed by transmission electron microscopy.

The interaction between Hsc70 and HttEx1Qn was assessed by plotting the inverse of assembly half-times against Hsc70 concentration, and fitting the plots to the following exponential function:

$1/t_{1/2} = A + (B\text{-}A)\bullet\exp(-c_{Hsc70}/EC_{50})$
where A is the asymptotic value of $1/t_{1/2}$, B is the value of $1/t_{1/2}$ without Hsc70, c_{Hsc70} is the concentration of Hsc70 in μM, and EC_{50} is the half maximal effective Hsc70 concentration.

Filter-trap assay and Western blotting. The presence of SDS-resistant material formed by HttEx1Q17 and HttEx1Q48 at the end of the aggregation reaction was assessed by a filter retardation assay (26) where 10 μL of each reaction were diluted in triplicate in 200 μL of 2% SDS, filtered through cellulose acetate membrane (0.2 μm pore size, Millipore Corp., Bedford, MA) using a 48-slot slot-blot filtration apparatus (GE Healthcare), and washed twice with 200 μL of 2% SDS. The cellulose acetate membranes were incubated with 3% skim milk, probed with a rabbit polyclonal anti-HttEx1Qn antibody we raised, and developed with the enzyme-coupled luminescence technique (ECL, Thermo Scientific) according to the recommendation of the manufacturer.

Fluorescence measurements. The binding of dansyl-Nt_{17} and its scrambled version to Hsc70 or soluble huntingtin's derived polypeptides was determined as follows. Dansyl-Nt_{17} and its scrambled version (1 μM) were co-incubated alone or with increasing concentrations of Hsc70 and/or HttEx1Q35, HttEx1Q35-ΔNt_{17} or Q35, for 10 min at room temperature. The fluorescence of the solution was then recorded on a Cary Eclipse Fluorescence Spectrophotometer (Varian Medical Systems Inc., California, USA) using the following settings: excitation wavelength = 340 nm; emission wavelength = 505 nm; excitation and emission slits = 2.5 and 10 nm, respectively.

Electron microscopy. Protein assemblies were examined by transmission electron microscopy (TEM) in a Jeol 1400 transmission electron microscope (Jeol SAS, Croissy-sur-Seine, France) following adsorption onto carbon-coated 200 mesh grids and negative staining with 1% uranyl acetate. The images were recorded with a Gatan Orius CCD camera (Gatan Inc., Pleasanton, CA, USA).

Fourier transformed infrared spectroscopy (FTIR). HttEx1Q25, HttEx1Q48, and HttEx1Q48 in the presence of equimolar concentrations of Hsc70 were assembled as described above. Fibrillar samples (5 mg) were spun at 16000g at 25°C for 20 min then extensively washed in D_2O. The spectra were recorded on a Jasco FT/IR-600 Plus spectrometer equipped with a nitrogen-cooled MTC detector, using the attenuated total reflectance mode. At total of 512 interferograms were collected at a resolution of 2 cm^{-1}. The sample chamber was continuously purged with CO_2-free air. The background consisted of D_2O and water vapor. All the spectra were baseline-corrected, smoothed and normalized prior to further data processing. As the same small quantity of Hsc70 was found in the pellet when the chaperone was incubated alone or in the presence of aggregating HttEx1Q48, the contribution of Hsc70 was subtracted from the spectra recorded for HttEx1Q48 fibrils formed in the presence of Hsc70.

Spectral analyses were performed using the Curvefitting Analysis software of the Spectra Manager package (Jasco). The amide I band (1575-1725 cm^{-1}) of each spectra was subjected to a fitting procedure using seven Gaussian distributions centered at the frequencies of well characterized secondary structures and lateral chains (27, 28). Each Gaussian was characterized by its frequency and an interval of given width. Each peak width was limited to 25 cm^{-1} while their heights were left free. The contribution of each curve to the amide I band was assessed by integrating the area under the curve and normalizing to the total area under the amide I band.

Circular dichroism. For CD measurements, the Nt_{17} peptide was dissolved in HFIP, aliquoted, stored after evaporation of HFIP under N_2 at -20°C and then resuspended at 2 mM in PBS. Far-UV CD spectra were recorded at 20 °C using a JASCO J-810 dichrograph equipped with a thermostated cell holder using a 0.1-cm path length quartz cuvette. Each spectrum was the average of 5 acquisitions recorded in the 260 – 195 nm range with 0.5-nm steps, a bandwidth of 1 nm, and a speed of 50 $nm.min^{-1}$. The spectra were buffer corrected.

Cross-linking and two-dimensional (2D) gel electrophoresis. HttEx1Q25 (50 μM) in the presence or the absence of Hsc70 (50 μM) was incubated for 1h at 37°C in 40 mM Hepes-OH, pH

7.5, 75 mM KCl, 100 mM imidazole, 5 mM $MgCl_2$, 1 mM ATP and 10% glycerol. The cross-linking reaction was performed at room temperature for 30 min using BS3-d0/d4 (5 mM), a homo-bifunctional sulfo-NHS ester cross-linker reagent with an 11.4 Å spacer arm (Pierce, Waltham, MA, USA). The reaction was terminated by addition of ammonium bicarbonate (50 mM).

200 µg of cross-linked proteins were resolved by 2D gel electrophoresis using 7cm pH 4–7 IPG strips (Biorad) and the ReadyPrep™ 2-D Starter Kit (Biorad) following the Biorad instruction manual. Briefly, the products of the cross-linking reactions were precipitated in cold acetone, resuspended in the Rehydration Buffer (Biorad) and loaded on a 7 cm pH 4-7 ReadyStrip IPG strip (Biorad). The first dimension was performed using the PROTEAN IEF system (BIORAD) after active rehydration. For the second dimension, reduced, alkylated and equilibrated strips were applied on an 8% Tris-Glycine SDS-PAGE running gel. 2D gels were stained with Coomassie blue.

Peptide preparation and NanoLC-Linear ion trap (LTQ)-Orbitrap mass spectrometry analysis. Cross-linked protein complexes spots separated by 2D-gel electrophoresis were excised and subjected to tryptic or GluC digestion using the Progest robot and the digested peptides were extracted as described previously (29). Tryptic peptides were analyzed by nanoLC-Linear ion trap (LTQ)-Orbitrap mass spectrometry analysis and the nanoLC-MS/MS data were processed as described previously (29), except that the data analysis included Lysine, Serine, Threonine, Tyrosine and the N-terminal amino acid residues as possible cross-linked sites (30) and that the cross-linker was BS3-d0 and BS3-d4. Briefly, nanoLC-MS data were deisotoped using the Decon2LS software (http://omics.pnl.gov/software/Decon2LS.php). The resulting csv files were further analyzed with viper (http://omics.pnl.gov/software/VIPER.php) (31) to identify, within the nanoLC-MS analysis, the d0/d4 peptide pairs presenting mass differences of 4.0247 Da as a signature of peptides that have reacted with one molecule of BS3-d0/d4. Mass modifications were set to 138.0681 Da and 142.0928 Da for BS3-d0 and BS3-d4 cross-linked peptides respectively. A list of peptide pairs with a maximum mass deviation of less than 10 ppm between the experimental mass and the theoretical mass of each possible cross-linked peptides was generated and used to identify the BS3-d0/d4 cross-linked peptides using their MS/MS spectra and the GPMAW (32) and xQuest (33) softwares. Finally, identification of cross-linked peptides and location of cross-linking sites were manually validated by comparison of the experimental masses and the theoretical masses of the d0/d4 ion fragments pairs calculated for each cross-linked peptide. The peptide pairs listed in Table 2 have a maximum mass deviation of less than 3 ppm.

In vivo seeding assays. We compared the nucleation capacities of HttEx1Q48 fibrils assembled in the absence or the presence of Hsc70 using the assay we established in reporter cell lines (10, 34). In summary, U2OS cells stably expressing soluble mCherry fluorescent protein fused to HttEx1Q25 (HttEx1Q25-ChFP) were grown in McCOY's 5A medium supplemented with 10% FBS, 2mM glutamine, 100 units/mL penicillin, 100 µg/mL streptomycin and 500 µg/mL G418 on poly-L-lysine-coated coverslips. After 48h the cells were treated with 0.5 µM of HttEx1Q48 fibrils (monomer concentration) assembled in the absence or the presence of equimolar concentrations of Hsc70. After 24h the coverslips were washed with PBS, and the amount of HttEx1Q25-ChFP fluorescent foci was determined by direct live-measurement of fluorescence and cell counting. Images were acquired on the AxioObserver Z1 epifluorescence microscope equipped with an Incubator chamber XL multi S1 RED LS (Carl Zeiss) and an Orca-R2 camera (Hamamatsu).

RESULTS

Aggregation of HttEx1Qn of different polyQ lengths. We first established a protocol to purify recombinant soluble HttEx1Qn from the fusion precursor MBP-TEV-HttEx1Qn-His. An additional purification step after cleavage by the MBP-TEV allowed us to recover soluble HttEx1Qn separate from both the carrier protein and the protease. This ensured that the different modifiers of aggregation used throughout this study would not be diverted from HttEx1Qn by the

MBP-TEV or the cleaved MBP moiety. We then characterized the aggregation of HttEx1Qn with polyQ stretches ranging from 17 to 48 residues (**Fig. 1A**). As HttEx1Qn fibrils bind poorly to thioflavin T, the fluorescent dye commonly used to follow amyloid aggregation, we monitored the kinetics of aggregation not only by thioflavin T binding but also by quantifying SDS-soluble or SDS-insoluble HttEx1Qn species by SDS-PAGE (**Fig. 1B,C**). The kinetics of aggregation obtained from these different probes were similar (**Fig. 1D**).

The kinetics of HttEx1Q17, HttEx1Q25, HttEx1Q30, HttEx1Q35, HttEx1Q41 and HttEx1Q48 (**Fig. 1A**) aggregation in physiological conditions and at identical concentrations are represented in **Figure 1E**. As expected the longer the polyQ, the faster HttEx1Qn aggregated. Remarkably, we found a highly significant inverse linear correlation between the polyQ length and the logarithm of the aggregation half-time (**Fig. 1F;** r^2=0.90; p=0.004). We ascertained that HttEx1Qn of non-pathological polyQ lengths, i.e. of less than 35 consecutive Gln, assembled into SDS-resistant fibrils whose conformation was similar to the one adopted by HttEx1Q48 fibrils (**Fig. 1G**). The amount of fibrillar, SDS-insoluble, material at steady state was yet variable, with a threshold between 25 and 30 consecutive Gln (**Fig. 1H**).

Effects of Hsc70 and its co-chaperones Hdj1 and Hdj2 on HttEx1Q48 aggregation. We examined the impact of Hsc70, in its active, functional form, and its co-chaperones on HttEx1Qn aggregation (**Fig. 2 and 3**). We systematically verified that all chaperones were functional. To this end, we assessed both luciferase refolding and ATP hydrolysis (**Fig. 2A,B** and **3A,B**). Increasing Hsc70 concentrations progressively slowed down the kinetics of HttEx1Q48 aggregation (**Fig. 2C-E**). The effect of Hsc70 was even greater in the absence of nucleotides (**Fig. 2E**). This is consistent with a canonical chaperone functioning. Indeed in the absence of nucleotide, Hsc70 binds client proteins and do not release them. In the presence of ATP and upon ATP hydrolysis, the Hsc70 client binding site cycles between an open and a closed conformation with simultaneous binding and release of client proteins. The affinity of Hsc70 for soluble HttEx1Q48 in its active, functional form was derived from the corresponding aggregation half-times: the observed EC_{50} was equal to 8 μM (**Fig. 2F**). Notably, Hsc70 neither incorporated within the fibrils nor bound preformed fibrils (**Fig. 2G-H**).

To add a further level of complexity, we assessed the effect of the Hsc70 co-chaperones Hdj1 and Hdj2, alone or in combination with Hsc70 (**Fig. 3**). While Hdj2 had a marginal effect on HttEx1Q48 aggregation, Hdj1 significantly affected the reaction (**Fig. 3C-E**). Moreover, Hdj1 and Hdj2 acted synergistically with Hsc70 in slowing HttEx1Q48 assembly. In each case the measured effect of Hdj1 or Hdj2 and Hsc70 was significantly larger than that of the sum of individual chaperones (**Fig. 3E,F**).

We then assessed the consequences of Hsc70 presence in HttEx1Q48 aggregation reactions on the resulting assemblies scaffold. HttEx1Q48 assemblies obtained in the presence of equimolar amounts of Hsc70 looked indistinguishable from those formed in the absence of the chaperone in the electron microscope (compare **Figs. 4A** and **1G,** right panel). To determine whether Hsc70 affects HttEx1Q48 fibrillar architecture, the secondary structure contents of fibrillar HttEx1Q25, HttEx1Q48 and HttEx1Q48 obtained in the presence of equimolar concentrations of Hsc70 were assessed by FTIR spectroscopy. Spectra deconvolution showed that all the fibrils contained the amide I bands characteristic of the amyloid structure, although to a different extent (**Table 1**). HttEx1Q25 and HttEx1Q48 fibrils had different secondary structure contents, with HttEx1Q48 being richer in amyloid structure, at the expense of non-amyloid β-sheets (**Table 1**). Remarkably, the FTIR spectra of the HttEx1Q48 fibrils formed in the absence or presence of Hsc70 were markedly different, the latter being more similar to the spectra of HttEx1Q25 fibrils (**Fig. 4B, Table 1**).

Finally, we assessed the functional properties of HttEx1Q48 fibrils formed in the absence or presence of Hsc70 using the nucleation assay we established in reporter cell lines (U2OS cells) expressing soluble HttEx1Q25-ChFP (10, 34). The endogenous HttEx1Q25-ChFP redistributed into fluorescent foci in 50% of cells exposed to HttEx1Q48 fibrils formed in the absence of Hsc70 whereas only 22% of cells exposed to identical

concentrations of HttEx1Q48 fibrils formed in the presence of Hsc70 exhibited puncta (**Fig. 4C**).

We conclude from these observations that the interaction of Hsc70 with the soluble forms of HttEx1Qn of pathological length conferred to the latter kinetics, structural and functional properties characteristic of HttEx1Qn of non-pathological lengths.

Hsc70 effects on HttEx1Qn assembly is independent from polyQ length. Chaperones from the Hsp70 family have been described to interact mostly with solvent-exposed hydrophobic patches on polypeptides (23, 24). Thus, one could wonder how Hsc70 recognizes the main culprit of HttEx1Q48 aggregation, *i.e.* the highly polar expanded polyglutamine stretch. To determine whether Hsc70 interacts with HttEx1Qn polyglutamine stretch, the kinetics of aggregation of HttEx1Q41, HttEx1Q35, HttEx1Q30, HttEx1Q25 and HttEx1Q17 with increasing concentrations of Hsc70 were monitored as for HttEx1Q48. Similarly to what we observed for HttEx1Q48, Hsc70 slowed down the aggregation of all the HttEx1Qn we tested (**Fig. 5A-E**). Hsc70 also reduced the quantity of SDS-insoluble species formed at steady state (**Fig. 5A-E**). We derived from the assembly kinetics the EC_{50} of the Hsc70-HttEx1Qn interactions. All the measured EC_{50} were comprised between 2 and 6 μM (**Fig. 5F-J**), *i.e.* in the range of the Hsc70-HttEx1Q48 interaction (**Fig. 2F**). The differences we observed were within the experimental errors and did not depend on polyQ stretch length. We conclude from these measurements that Hsc70 slows down the aggregation of HttEx1Qn in a polyQ-length independent manner.

Hsc70 interacts with the N-terminal flank of HttEx1Qn. The fact that Hsc70 interacts to a similar extend with HttEx1Qn displaying polyQ stretches ranging from 17 to 48 Gln residues suggests it recognizes the polyQ adjacent flanks, *e.g.* either the 17-residues long N-terminal portion (Nt_{17}) or the Pro-rich, 53-residues long C-terminal portion (Ct_{53}) of HttEx1Qn. We first focused on Nt_{17} as it influences the *in vivo* aggregation of the huntingtin protein in many different ways (35–38), and is proposed to initiate the aggregation of HttEx1Qn *in vitro* (see (39) for a review). To determine whether Hsc70 could interact with HttEx1Qn through Nt_{17} we compared the aggregation of HttEx1Q35-ΔNt_{17} and Q35 (**Fig. 1A**) in the absence and the presence of Hsc70. In contrast to what was observed for HttEx1Qn, Hsc70 had no effect on the kinetics of aggregation of HttEx1Q35-ΔNt_{17} or Q35 (**Fig. 6A,B**).

To further demonstrate that Hsc70 interacts indeed with Nt_{17}, the effect of Hsc70 on HttEx1Q48 aggregation in the presence or the absence of free Nt_{17} was compared (**Fig. 6C**). As reported previously (40, 41), free Nt_{17} slowed down the aggregation of HttEx1Q48. The observed inhibitory effect was lifted when Nt_{17} was pre-incubated with Hsc70 prior to addition to HttEx1Q48 (**Fig. 6C,D**). Thus, Hsc70 and Nt_{17} had antagonistic effects on HttEx1Q48 aggregation, suggesting that Hsc70 sequesters Nt_{17}, thus reducing its free concentration in solution. We next assessed Nt_{17} interaction with Hsc70 using a fluorescent Nt_{17} peptide. The specific fluorescence of N-terminally dansyl labeled Nt_{17} (**Fig. 1A**) increased upon addition of increasing concentrations Hsc70 (**Fig. 6E**). The increased fluorescence intensity indicated that Nt_{17} peptide was in a more hydrophobic environment following its interaction with Hsc70. A scrambled version of dansyl-Nt_{17} interacted to a lesser extent with Hsc70, and free dansyl did not interact at all (**Fig. 6E**). The fact that scrambled dansyl-Nt_{17} still binds to Hsc70, although to a lesser extent than normal dansyl-Nt_{17} is certainly due to Hsc70 ability to binds to most peptides composed of non polar amino acids and limited selectivity (23). Finally we saw a competition between Hsc70 and HttEx1Q35 for dansyl-Nt_{17} binding (**Fig. 6E**), in agreement with the competition between Hsc70 and Nt_{17} for HttEx1Q35 reported in **Figure 6C**. These results suggest that Hsc70 binds Nt_{17} within HttEx1Qn.

We next mapped the surface interfaces between Hsc70 and HttEx1Qn using chemical cross-linking with the homo-bifunctional NHS-ester BS3 cross-linker and mass-spectrometry, using a strategy that we developed previously to assess Hsc70 interaction with another client protein and described in detail in reference (29). Hsc70 interacts in a similar way with all the soluble forms of HttEx1Qn we tested (**Fig. 5**). We therefore used HttEx1Q25 in the cross-linking studies as despite being able to assemble into fibrils it remains soluble for sufficient time in

solution to allow cross-linking (see **Fig. 1E**). Hsc70 and HttEx1Q25 were first allowed to interact for 1 hour at 37°C and the complexes were cross-linked with a mixture of non-deuterated (d0) and deuterated (d4) NHS-ester BS3. The resulting complexes were resolved by two-dimensional gel electrophoresis (**Fig. 7A**), trypsin digested in the gel, and the identity of the resulting peptides was determined by nanoLC-MS/MS LTQ-Orbitrap and both MS and MS/MS data analysis as described in the Experimental Procedures and in reference (29). Seven Hsc70-HttEx1Q25 cross-links were identified (**Table 2**). Hsc70 lysine residues involved in the interaction with HttEx1Q25 are mapped on the three-dimensional model of Hsc70 client polypeptides binding site we built (29). The identification of two representative cross-links is illustrated in **Figure 7C-H**. The MS spectra of the triple charged Hsc70 494-500 - HttEx1Q25 1-8 and triple charged Hsc70 551-561- HttEx1Q25 9-17 cross-links with m/z 579.6293 / 580.9713 and 813.1016 / 814.4431 ion pairs for the BS3-d0 and BS3-d4 peptides, are presented in **Figure 7C** and **F**, respectively. The LTQ-Orbitrap fragmentation mass spectra of the BS3-d4 ions with m/z 580.97 and BS3-d0 with m/z 813.4362 are shown in the **Figure 7D** and **G**, respectively. Finally, the Hsc70 and HttEx1Q25 sequences of the cross-linked peptides identified through y and b fragment ions are displayed in **Figure 7E** and **H**. The complete list of identified cross-links involving Hsc70 452-469, 494-500, 551-561, 558-567 and 558-569 and HttEx1Q25 1-8 and 9-17 is given in **Table 2**. All the cross-linked lysine residues identified within Hsc70 (K458, 497, 557 and 561) are situated within its client protein binding domain. All of the cross-linked residues identified within HttEx1Q25 (G1, T5 and K11) are in HttEx1Q25 Nt_{17}. Thus, Hsc70 binds unequivocally HttEx1Qn through the polypeptide that flanks N-terminally the polyQ stretch.

Hsc70 binding to the N-terminal flank of HttEx1Qn shields a sequence essential for the aggregation process. HttEx1Qn Nt flank has been reported to impact aggregation *in vitro,* possibly through the establishment of homotypic Nt_{17}-Nt_{17} interactions that would allow the coalescence of the HttEx1Qn molecules (39). Free Nt_{17} yields CD spectra typical of coiled-coil structures in solution (**Fig. 9A**). To assess the existence of Nt_{17}-Nt_{17} interactions within aggregating HttEx1Qn, HttEx1Q25 was allowed to oligomerize for 1h at 37°C. The oligomers were cross-linked with a mixture of non-deuterated (d0) and deuterated (d4) NHS-ester BS3, resolved by SDS-PAGE, trypsin-digested in the gel, and the identity of the resulting peptides was determined by nanoLC-MS/MS LTQ-Orbitrap analyses (29).

A single inter-molecular cross-link was identified as illustrated in **Figure 8A-C**. The MS spectra of the triple charged HttEx1Q25-HttEx1Q25 cross-links with m/z 905.4527 / 907.4648 ion pairs for the BS3-d0 and BS3-d4 peptides, is shown in **Figure 8A**. The LTQ-Orbitrap fragmentation mass spectra of the BS3-d0 and BS3-d4 ions are shown in the **Figure 8B** (upper and bottom spectra, respectively). Finally, the HttEx1Q25 1-8 -HttEx1Q25 1-8 sequence of the cross-linked peptide identified through y and b fragment ions is presented in **Figure 8C**. HttEx1Q25 is cross-linked to another HttEx1Q25 through the N-terminal residue of its Nt flank. These results show unequivocally that HttEx1Qn molecules interact during fibrils formation through their moiety that flanks N-terminally the polyQ stretch.

Finally, we assessed the specific contribution of these Nt_{17}-Nt_{17} interactions to the aggregation process. HttEx1Q35 aggregates faster than variants of similar polyQ length devoid of Nt_{17} (Q35 or HttEx1Q35-ΔNt_{17}), suggesting that the Nt_{17} contributes to the aggregation process of HttEx1Qn (**Fig. 8D**). To demonstrate that this is indeed the case, we monitored the aggregation of HttEx1Q35, Q35 and HttEx1Q35-ΔNt_{17} with increasing concentration of free Nt_{17} added to compete with the Nt flank when present. While free Nt_{17} slowed down the aggregation of HttEx1Q35 (**Fig. 8E**), it neither impacted HttEx1Q35-ΔNt_{17} (**Fig. 8F**) nor Q35 (**Fig. 8G**) aggregation. Further demonstration of direct interaction between Nt_{17} and HttEx1Q35 came from the increase of fluorescence intensity upon incubation of dansyl-Nt_{17} with HttEx1Q35, while no such increase was observed upon incubation with HttEx1Q35-ΔNt_{17} or Q35 (**Fig. 6E**). Altogether these observations demonstrate that free Nt_{17} binds to HttEx1Q35 and interfere in a competitive manner with the initial step of HttEx1Q35 fibrils formation.

We conclude from our observations that HttEx1Qn N-terminal flanks drive the coalescence of the molecules during the early stages of assembly.

DISCUSSION

Molecular chaperones are the first line of defense against the aggregation of the cellular proteins involved in neurodegenerative diseases. The guardian activity of chaperones is based on their ability to bind stretches of aggregation-prone hydrophobic residues that are exposed to the solvent in unstructured or misfolded proteins (23, 24). An intriguing question in this respect was whether the alleviating effect of Hsc70 on the toxicity of the polyQ-expanded huntingtin protein observed *in vivo* (15, 17, 18, 42, 43) reflected or not a presumably unfavorable direct interaction between the chaperone and the aggregation-prone polyQ stretch.

Here we define the molecular mechanism by which human Hsc70 interferes with the aggregation of recombinant HttEx1Qn. We show that Hsc70 binds directly to soluble but not fibrillar HttEx1Qn and that the interaction of soluble HttEx1Qn with Hsc70 affects not only the assembly kinetic into fibrils but also the fibrillar scaffold and its functional properties. We next unequivocally demonstrate that Hsc70 binds to a sequence adjacent to the polyQ stretch and map this interaction at the residue-level. Finally, we elucidate the primary role of this sequence in the aggregation of HttEx1Qn, thus clarifying both the modes of Hsc70 action and HttEx1Qn molecules coalescence prior to their assembly into fibrils.

Aggregation of HttEx1Qn of pathological and non-pathological polyQ lengths: the threshold issue. We first characterized the aggregation of HttEx1Qn of pathological (n=48, 41 or 35) and non-pathological lengths (n=30, 25 or 17). For the first time to our knowledge, HttEx1Qn of non-pathological polyQ lengths is shown to form fibrils presenting amyloid-like characteristics. The aggregation of HttEx1Qn with short and long polyQ stretches only differed by their assembly kinetics. The lag phases preceding assembly and the elongation slopes varied with the polyQ stretch length. The shorter the polyQ stretch, the longer was the nucleation phase and the lower was the elongation slope. As reported previously for naked synthetic Qn peptides (11, 44), we show a strong exponential inverse correlation between the length of the polyQ stretch and the kinetics of HttEx1Qn aggregation, with no apparent threshold between pathological (Q≥35) and non pathological (Q≤30) polyQ stretch lengths. The same exponential inverse correlation is observed between the length of huntingtin alleles (Q≥40) and the age-of-onset of the disease (45–47), as if the kinetics of huntingtin aggregation would explain by its own the variations in the ages-of-onset. If this is indeed the case, one could speculate that short polyQ stretch lengths are non-pathological only because of our life span. By extrapolating the epidemic data from Wexler *et al* (47) and considering a stretch of 17 Gln residues (the most abundant allele in the human population), we conjecture that we would all develop HD if we would live till 145 years.

We sampled the SDS-resistance of HttEx1Qn of different polyQ stretch lengths and saw differences between short and long polyQ stretches, as observed previously (48). Correspondingly we observed a clear difference between the secondary structure content of fibrils formed by HttEx1Q25 and HttEx1Q48 as determined by FTIR, with the latter being richer in amyloid-like structures. Previously published structural analyses of polyQ fibrils performed mostly on synthetic Qn showed no similar structural transition (49–51). However, one group reported differences in the FTIR spectra of fibrils from recombinant ataxin 3 containing 24 or 55 glutamines (52). The apparent discrepancy between results obtained using synthetic Qn peptides and recombinant polyQ proteins highlight the importance of polyQ stretches natural context.

Finally, we note that the threshold we observed in the SDS-resistance of the fibrils lies between 25 and 30 glutamine, when individuals carrying a huntingtin allele of less than 35 glutamines are considered healthy. One first obvious explanation is that *in vitro* aggregation of recombinant polypeptides cannot recapitulate the whole toxic process that takes place in a living organism. However recent studies show that individuals with intermediate polyQ lengths (i.e 27-35 glutamines) display statistically significant clinical symptoms (53, 54), and cases of autopsy-

proven HD with a polyQ stretch shorter than 30 have been reported (55, 56). The combination of these epidemiological data and our structural and kinetic results suggests that huntingtin alleles of intermediate polyQ lengths can indeed become pathological if an individual lives for long enough.

Structure-function relationship for HttEx1Qn fibrils. Hsc70, in its active, functional form, slows down HttEx1Qn assembly into fibrils. The resulting fibrils are indistinguishable from those obtained in the absence of Hsc70 based on electron micrographs. However, HttEx1Qn interaction with Hsc70 has consequences on the fibrillar scaffold. HttEx1Qn fibrils assembled in the presence of Hsc70 have the secondary structure content and the functional properties of fibrils assembled from HttEx1Qn with non-pathological polyQ lengths. Our results establish a structure-function relationship for HttEx1Qn fibrils, since different secondary structures of fibrils exhibit different infectious properties. We recently demonstrated that in the cases of both α-Synuclein and HttEx1Qn, the fibrils are the most toxic species to the cells (57). Hence, the Hsc70-mediated changes in pathologic HttEx1Qn fibrils structural and functional properties is of importance as it suggests that increased availability of Hsc70 *in vivo* may contribute to the clearance of fibrils and represent a therapeutic avenues.

A detailed mechanism of action for Hsc70. We used a combination of different and complementary approaches to unveil the molecular mechanism by which Hsc70 mitigates HttEx1Qn aggregation. Multiple evidence show that Hsc70 binds to the 17-residue long N-terminal portion of the HttEx1Qn: (*i*) the effect of Hsc70 on HttEx1Qn aggregation does not depend on polyQ length but on the presence of the polyQ stretch N-terminal flank; (*ii*) Hsc70 binds fluorescently labeled free Nt_{17}; (*iii*) free Nt_{17} titrates the effect of Hsc70 on HttEx1Qn aggregation; and finally (*iv*) the residues involved in Hsc70-HttEx1Q25 interaction are all located in HttEx1Q25 N-terminal flank as revealed by our cross-linking studies. We cannot exclude that Hsc70 binds to another portion of the HttEx1Qn. This is however highly unlikely as we subjected Hsc70-HttEx1Qn to GluC digestion and detected no additional crosslinks. There is currently no specific cross-linker that can react with a Gln residue, yet the fact that the Hsc70-HttEx1Qn interaction is independent from polyQ length while dependent on HttEx1Qn N-terminal flank argues against a direct Hsc70-polyQ interaction.

Binding to a portion of the sequence or a domain adjacent to a polyQ tract may not be a prerogative of Hsc70. Hsp100 VCP, αB-crystallin (58, 59), TRiC, Ssa1, DnaJ, DnaK or Hsp90 (42, 60–62) bind ataxin 3 or HttEx1Qn with normal or expanded polyQ stretch lengths in a similar way. However to the best of our knowledge this is the first time that a chaperone-binding site is unequivocally mapped at a residue-level precision to a flanking sequence of a polyQ-containing protein, bringing insight into the aggregation process of such proteins. This underlies the power and the potential of the cross-link-MS approach we developed previously (29, 63). In this respect, it is noteworthy that Hsc70 binds α-Synuclein (29) and HttEx1Qn (this work) through the same residues within the substrate-binding domain. Other chaperones such as DNAJB6 bind directly the polyQ tract as this chaperone has been shown to prevent the aggregation of Qn much more efficiently than HttEx1Qn of the same polyQ length (64).

The N-terminal 17 amino acid residues of HttEx1Qn and aggregation. The findings that (i) HttEx1Qn aggregate faster than HttEx1Qn-ΔNt_{17}, (ii) Nt_{17} affects HttEx1Qn aggregation but not that of Qn and HttEx1Qn-ΔNt_{17}, and *(iii)* intermolecular Nt_{17}-Nt_{17} interactions are established in the early stages of HttEx1Qn aggregation, indicate that the Nt_{17} flank of HttEx1Qn plays a critical role in the aggregation process.

Beside being involved in (i) cytosolic retention (35, 36), (ii) interaction with membranous structures (36, 38), and (iii) HD progression following post-translational modifications (35, 37, 65), huntingtin's Nt_{17} flank seems to influence huntingtin aggregation. Studies aimed at documenting the exact role of huntingtin's Nt_{17} flank yielded so far contradictory observations. The effect of free Nt_{17} on the aggregation of HttEx1Qn, or a synthetic peptide almost reproducing HttEx1Qn, had either anti-

(40, 41) or pro- (60) aggregation properties. In addition, Nt_{17} either accelerated (60) nor had effect (40, 41) on the aggregation of HttEx1Qn-ΔNt_{17}. Our results unequivocally demonstrate that HttEx1Qn N-terminal 17 amino acid residues play a critical role in HttEx1Qn assembly.

Two scenarios were proposed for the pathogenic aggregation of polyQ-containing proteins. In all cases aggregation was proposed to be a two-step process. In a set of models, the polyQ stretch drives primarily aggregation and the flanking regions have either counter or no effects (66, 67). In another set of models, it is the coalescence of polyQ stretches-flanking regions that drives the coalescence of the polyQ-containing proteins with secondary consolidation of the assemblies by the rearrangement of the polyQ stretches into amyloid-like structures (68, 69). In the later cases, further studies suggested that the polyQ stretches-flanking regions polymerize *via* the formation of coiled-coils (69). Our findings support the latter scenario with HttEx1Qn N-terminal flank driven formation of in register coiled-coils. Indeed we demonstrated that HttEx1Qn molecules are cross-linked early on during the assembly process through the N-terminal residue of their Nt flanks. In addition, free Nt_{17} forms a coiled-coil structure in solution (**Fig. 9A**). Finally the cross-linker BS3, which spacer arm length is 11Å imposes structural constraints indicative of the arrangement of HttEx1Qn molecules within on-assembly pathway HttEx1Qn oligomeric species. This in register arrangement is schematized in **Figure 9B** for HttEx1Qn 17 N-terminal amino acid residues in a wheel structural representation.

The overall contribution of HttEx1Qn Nt_{17} flank to the aggregation process and the interference of Hsc70 within the process is schematized in **Figure 9C,D**. HttEx1Qn molecules coalescence, in the early stages of assembly, is driven by homotypic interactions between Nt_{17}. PolyQ-polyQ interactions stabilize the nuclei and certainly contribute to fibrils elongation at a later stage (**Fig. 9C**). Hsc70 sequesters HttEx1Qn molecules after binding their Nt_{17} and interferes with HttEx1Qn coalescence. This impacts the kinetics of fibril formation. This also yields distinct HttEx1Qn folding intermediates, given that the resulting fibrils display lower ß-sheet content, resistance to SDS and nucleation/infectious propensities (**Fig. 9D**).

These modifications are likely to have biological relevance. By establishing the critical role of the 17 N-terminal amino acid residues of HttEx1Qn in its aggregation process, bringing insights into the geometry of the on-assembly pathway HttEx1Qn oligomeric species and identifying Hsc70 amino acid stretches that interact with HttEx1Qn we lay the foundations of future therapeutic strategies. Indeed, the results we report pave the way for the design of therapeutic tools in HD targeting HttEx1Qn aggregation. Our findings may lead to the design of two classes of therapeutic tools: peptides derived from the N-terminal flank of HttEx1Qn that interfere with HttEx1Qn Nt flank-driven coalescence or peptides derived from Hsc70 client protein binding site that interact with HttEx1Qn in a manner similar to the entire chaperone and (i) slow down aggregation and/or (ii) yield fibrils with limited resistance to the cellular clearance machinery and/or seeding propensity.

REFERENCES

1. Graham, R. K., Deng, Y., Slow, E. J., Haigh, B., Bissada, N., Lu, G., Pearson, J., Shehadeh, J., Bertram, L., Murphy, Z., Warby, S. C., Doty, C. N., Roy, S., Wellington, C. L., Leavitt, B. R., Raymond, L. A., Nicholson, D. W., and Hayden, M. R. (2006) Cleavage at the Caspase-6 Site Is Required for Neuronal Dysfunction and Degeneration Due to Mutant Huntingtin. *Cell* **125**, 1179–1191

2. Sieradzan, K. A., Mechan, A. O., Jones, L., Wanker, E. E., Nukina, N., and Mann, D. M. (1999) Huntington's disease intranuclear inclusions contain truncated, ubiquitinated huntingtin protein. *Exp. Neurol.* **156**, 92–99

3. DiFiglia, M., Sapp, E., Chase, K. O., Davies, S. W., Bates, G. P., Vonsattel, J. P., and Aronin, N. (1997) Aggregation of huntingtin in neuronal intranuclear inclusions and dystrophic neurites in brain. *Science* **277**, 1990–1993

4. Schulte, J., Littleton, J. T., and J., S. (2011) The biological function of the Huntingtin protein and its relevance to Huntington's Disease pathology. *Curr Trends Neurol* **5**, 65–78

5. Paulson, H. L., Bonini, N. M., and Roth, K. A. (2000) Polyglutamine disease and neuronal cell death. *Proc. Natl. Acad. Sci. U. S. A.* **97**, 12957–12958

6. Finkbeiner, S. (2011) Huntington's Disease. *Cold Spring Harb. Perspect. Biol.* **3**

7. Rubinsztein, D. C. (2002) Lessons from animal models of Huntington's disease. *Trends Genet.* **18**, 202–209

8. Scherzinger, E., Sittler, A., Schweiger, K., Heiser, V., Lurz, R., Hasenbank, R., Bates, G. P., Lehrach, H., and Wanker, E. E. (1999) Self-assembly of polyglutamine-containing huntingtin fragments into amyloid-like fibrils: implications for Huntington's disease pathology. *Proc. Natl. Acad. Sci. U. S. A.* **96**, 4604–4609

9. Brundin, P., Melki, R., and Kopito, R. (2010) Prion-like transmission of protein aggregates in neurodegenerative diseases. *Nat. Rev. Mol. Cell Biol.* **11**, 301–307

10. Ren, P.-H., Lauckner, J. E., Kachirskaia, I., Heuser, J. E., Melki, R., and Kopito, R. R. (2009) Cytoplasmic penetration and persistent infection of mammalian cells by polyglutamine aggregates. *Nat. Cell Biol.* **11**, 219–225

11. Chen, S., Berthelier, V., Yang, W., and Wetzel, R. (2001) Polyglutamine aggregation behavior in vitro supports a recruitment mechanism of cytotoxicity. *J. Mol. Biol.* **311**, 173–182

12. Bhattacharyya, A., Thakur, A. K., Chellgren, V. M., Thiagarajan, G., Williams, A. D., Chellgren, B. W., Creamer, T. P., and Wetzel, R. (2006) Oligoproline effects on polyglutamine conformation and aggregation. *J. Mol. Biol.* **355**, 524–535

13. Sivanandam, V. N., Jayaraman, M., Hoop, C. L., Kodali, R., Wetzel, R., and van der Wel, P. C. A. (2011) The aggregation-enhancing huntingtin N-terminus is helical in amyloid fibrils. *J. Am. Chem. Soc.* **133**, 4558–4566

14. Kelley, N. W., Huang, X., Tam, S., Spiess, C., Frydman, J., and Pande, V. S. (2009) The Predicted Structure of the Headpiece of the Huntingtin Protein and Its Implications on Huntingtin Aggregation. *J. Mol. Biol.* **388**, 919–927

15. Rujano, M. A., Kampinga, H. H., and Salomons, F. A. (2007) Modulation of polyglutamine inclusion formation by the Hsp70 chaperone machine. *Exp. Cell Res.* **313**, 3568–3578

16. Hay, D. G., Sathasivam, K., Tobaben, S., Stahl, B., Marber, M., Mestril, R., Mahal, A., Smith, D. L., Woodman, B., and Bates, G. P. (2004) Progressive decrease in chaperone protein levels in a mouse model of Huntington's disease and induction of stress proteins as a therapeutic approach. *Hum. Mol. Genet.* **13**, 1389–1405

17. Tagawa, K., Marubuchi, S., Qi, M.-L., Enokido, Y., Tamura, T., Inagaki, R., Murata, M., Kanazawa, I., Wanker, E. E., and Okazawa, H. (2007) The induction levels of heat shock protein 70 differentiate the vulnerabilities to mutant huntingtin among neuronal subtypes. *J. Neurosci.* **27**, 868–880

18. Chan, H. Y., Warrick, J. M., Gray-Board, G. L., Paulson, H. L., and Bonini, N. M. (2000) Mechanisms of chaperone suppression of polyglutamine disease: selectivity, synergy and modulation of protein solubility in Drosophila. *Hum. Mol. Genet.* **9**, 2811–2820

19. Olshina, M. A., Angley, L. M., Ramdzan, Y. M., Tang, J., Bailey, M. F., Hill, A. F., and Hatters, D. M. (2010) Tracking mutant huntingtin aggregation kinetics in cells reveals three major populations that include an invariant oligomer pool. *J. Biol. Chem.* **285**, 21807–21816

20. Zhou, H., Li, S. H., and Li, X. J. (2001) Chaperone suppression of cellular toxicity of huntingtin is independent of polyglutamine aggregation. *J. Biol. Chem.* **276**, 48417–48424

21. Meriin, A. B., Zhang, X., He, X., Newnam, G. P., Chernoff, Y. O., and Sherman, M. Y. (2002) Huntington toxicity in yeast model depends on polyglutamine aggregation mediated by a prion-like protein Rnq1. *J. Cell Biol.* **157**, 997–1004

22. Yu, A., Shibata, Y., Shah, B., Calamini, B., Lo, D. C., and Morimoto, R. I. (2014) Protein aggregation can inhibit clathrin-mediated endocytosis by chaperone competition. *Proc. Natl. Acad. Sci. U. S. A.* **111**, E1481–E1490

23. Rüdiger, S., Germeroth, L., Schneider-Mergener, J., and Bukau, B. (1997) Substrate specificity of the DnaK chaperone determined by screening cellulose-bound peptide libraries. *EMBO J.* **16**, 1501–1507

24. Rüdiger, S., Schneider-Mergener, J., and Bukau, B. (2001) Its substrate specificity characterizes the DnaJ co-chaperone as a scanning factor for the DnaK chaperone. *EMBO J.* **20**, 1042–1050

25. Pemberton, S., Madiona, K., Pieri, L., Kabani, M., Bousset, L., and Melki, R. (2011) Hsc70 protein interaction with soluble and fibrillar alpha-synuclein. *J Biol Chem* **286**, 34690–34699

26. Wanker, E. E., Scherzinger, E., Heiser, V., Sittler, A., Eickhoff, H., and Lehrach, H. (1999) Membrane filter assay for detection of amyloid-like polyglutamine-containing protein aggregates. *Methods Enzymol.* **309**, 375–386

27. Zurdo, J., Guijarro, J. I., and Dobson, C. M. (2001) Preparation and characterization of purified amyloid fibrils. *J. Am. Chem. Soc.* **123**, 8141–8142

28. Seshadri, S., Khurana, R., and Fink, A. L. (1999) Fourier transform infrared spectroscopy in analysis of protein deposits. *Methods Enzymol.* **309**, 559–576

29. Redeker, V., Pemberton, S., Bienvenut, W., Bousset, L., and Melki, R. (2012) Identification of protein interfaces between alpha-synuclein, the principal component of Lewy bodies in Parkinson disease, and the molecular chaperones human Hsc70 and the yeast Ssa1p. *J Biol Chem* **287**, 32630–32639

30. Mädler, S., Bich, C., Touboul, D., and Zenobi, R. (2009) Chemical cross-linking with NHS esters: a systematic study on amino acid reactivities. *J. Mass Spectrom.* **44**, 694–706

31. Zimmer, J. S. D., Monroe, M. E., Qian, W., and Smith, R. D. (2006) Advances in Proteomics Data Analysis and Display Using an Accurate Mass and Time Tag Approach. *Mass Spectrom. Rev.* **25**, 450–482

32. Peri, S., Steen, H., and Pandey, A. (2001) GPMAW – a software tool for analyzing proteins and peptides. *Trends Biochem. Sci.* **26**, 687–689

33. Rinner, O., Seebacher, J., Walzthoeni, T., Mueller, L. N., Beck, M., Schmidt, A., Mueller, M., and Aebersold, R. (2008) Identification of cross-linked peptides from large sequence databases. *Nat. Methods* **5**, 315–318

34. Trevino, R. S., Lauckner, J. E., Sourigues, Y., Pearce, M. M., Bousset, L., Melki, R., and Kopito, R. R. (2012) Fibrillar structure and charge determine the interaction of polyglutamine protein aggregates with the cell surface. *J. Biol. Chem.* **287**, 29722–29728

35. Steffan, J. S., Agrawal, N., Pallos, J., Rockabrand, E., Trotman, L. C., Slepko, N., Illes, K., Lukacsovich, T., Zhu, Y.-Z., Cattaneo, E., Pandolfi, P. P., Thompson, L. M., and Marsh, J. L. (2004) SUMO modification of Huntingtin and Huntington's disease pathology. *Science* **304**, 100–104

36. Atwal, R. S., Xia, J., Pinchev, D., Taylor, J., Epand, R. M., and Truant, R. (2007) Huntingtin has a membrane association signal that can modulate huntingtin aggregation, nuclear entry and toxicity. *Hum. Mol. Genet.* **16**, 2600–2615

37. Atwal, R. S., Desmond, C. R., Caron, N., Maiuri, T., Xia, J., Sipione, S., and Truant, R. (2011) Kinase inhibitors modulate huntingtin cell localization and toxicity. *Nat. Chem. Biol.* **7**, 453–460

38. Rockabrand, E., Slepko, N., Pantalone, A., Nukala, V. N., Kazantsev, A., Marsh, J. L., Sullivan, P. G., Steffan, J. S., Sensi, S. L., and Thompson, L. M. (2007) The first 17 amino acids of Huntingtin modulate its sub-cellular localization, aggregation and effects on calcium homeostasis. *Hum. Mol. Genet.* **16**, 61–77

39. Wetzel, R. (2012) Physical chemistry of polyglutamine: Intriguing tales of a monotonous sequence. *J. Mol. Biol.* **421**, 466–490

40. Mishra, R., Jayaraman, M., Roland, B. P., Landrum, E., Fullam, T., Kodali, R., Thakur, A. K., Arduini, I., and Wetzel, R. (2012) Inhibiting the nucleation of amyloid structure in a huntingtin fragment by targeting α-helix-rich oligomeric intermediates. *J. Mol. Biol.* **415**, 900–917

41. Jayaraman, M., Mishra, R., Kodali, R., Thakur, A. K., Koharudin, L. M. I., Gronenborn, A. M., and Wetzel, R. (2012) Kinetically competing huntingtin aggregation pathways control amyloid polymorphism and properties. *Biochemistry* **51**, 2706–2716

42. Muchowski, P. J., Schaffar, G., Sittler, A., Wanker, E. E., Hayer-Hartl, M. K., and Hartl, F. U. (2000) Hsp70 and hsp40 chaperones can inhibit self-assembly of polyglutamine proteins into amyloid-like fibrils. *Proc. Natl. Acad. Sci. U. S. A.* **97**, 7841–7846

43. Guzhova, I. V, Lazarev, V. F., Kaznacheeva, A. V, Ippolitova, M. V, Muronetz, V. I., Kinev, A. V, and Margulis, B. a (2011) Novel mechanism of Hsp70 chaperone-mediated prevention of polyglutamine aggregates in a cellular model of huntington disease. *Hum. Mol. Genet.* **20**, 3953–3963

44. Landrum, E., and Wetzel, R. (2014) Biophysical underpinnings of the repeat length dependence of polyglutamine amyloid formation. *J. Biol. Chem.* **289**, 10254–10260

45. Andrew, S. E., Goldberg, Y. P., Kremer, B., Telenius, H., Theilmann, J., Adam, S., Starr, E., Squitieri, F., Lin, B., and Kalchman, M. A. (1993) The relationship between trinucleotide (CAG) repeat length and clinical features of Huntington's disease. *Nat. Genet.* **4**, 398–403

46. Brinkman, R. R., Mezei, M. M., Theilmann, J., Almqvist, E., and Hayden, M. R. (1997) The likelihood of being affected with Huntington disease by a particular age, for a specific CAG size. *Am. J. Hum. Genet.* **60**, 1202–1210

47. Wexler, N. S., Lorimer, J., Porter, J., Gomez, F., Moskowitz, C., Shackell, E., Marder, K., Penchaszadeh, G., Roberts, S. A., Gayán, J., Brocklebank, D., Cherny, S. S., Cardon, L. R., Gray, J., Dlouhy, S. R., Wiktorski, S., Hodes, M. E., Conneally, P. M., Penney, J. B., Gusella, J., Cha, J.-H., Irizarry, M., Rosas, D., Hersch, S., Hollingsworth, Z., MacDonald, M., Young, A. B., Andresen, J. M., Housman, D. E., De Young, M. M., Bonilla, E., Stillings, T., Negrette, A., Snodgrass, S. R., Martinez-Jaurrieta, M. D., Ramos-Arroyo, M. A., Bickham, J., Ramos, J. S., Marshall, F., Shoulson, I., Rey, G. J., Feigin, A., Arnheim, N., Acevedo-Cruz, A., Acosta, L., Alvir, J., Fischbeck, K., Thompson, L. M., Young, A., Dure, L., O'Brien, C. J., Paulsen, J., Brickman, A., Krch, D., Peery, S., Hogarth, P., Higgins, D. S., and Landwehrmeyer, B. (2004) Venezuelan kindreds reveal that genetic and environmental factors modulate Huntington's disease age of onset. *Proc. Natl. Acad. Sci. U. S. A.* **101**, 3498–3503

48. Klein, F. A. C., Pastore, A., Masino, L., Zeder-Lutz, G., Nierengarten, H., Oulad-Abdelghani, M., Altschuh, D., Mandel, J. L., and Trottier, Y. (2007) Pathogenic and Non-pathogenic Polyglutamine Tracts Have Similar Structural Properties: Towards a Length-dependent Toxicity Gradient. *J. Mol. Biol.* **371**, 235–244

49. Thakur, A. K., Jayaraman, M., Mishra, R., Thakur, M., Chellgren, V. M., Byeon, I.-J. L., Anjum, D. H., Kodali, R., Creamer, T. P., Conway, J. F., Gronenborn, A. M., and Wetzel, R. (2009)

Polyglutamine disruption of the huntingtin exon 1 N terminus triggers a complex aggregation mechanism. *Nat. Struct. Mol. Biol.* **16**, 380–389

50. Sharma, D., Shinchuk, L. M., Inouye, H., Wetzel, R., and Kirschner, D. A. (2005) Polyglutamine homopolymers having 8-45 residues form slablike beta-crystallite assemblies. *Proteins* **61**, 398–411

51. Kurouski, D., Kar, K., Wetzel, R., Dukor, R. K., Lednev, I. K., and Nafie, L. A. (2013) Levels of supramolecular chirality of polyglutamine aggregates revealed by vibrational circular dichroism. *FEBS Lett.* **587**, 1638–1643

52. Natalello, A., Frana, A. M., Relini, A., Apicella, A., Invernizzi, G., Casari, C., Gliozzi, A., Doglia, S. M., Tortora, P., and Regonesi, M. E. (2011) A major role for side-chain polyglutamine hydrogen bonding in irreversible ataxin-3 aggregation. *PLoS One* **6**, e18789

53. Ha, A. D., and Jankovic, J. (2011) Exploring the correlates of intermediate CAG repeats in Huntington disease. *Postgrad. Med.* **123**, 116–121

54. Killoran, A., Biglan, K. M., Jankovic, J., Eberly, S., Kayson, E., Oakes, D., Young, A. B., and Shoulson, I. (2013) Characterization of the Huntington intermediate CAG repeat expansion phenotype in PHAROS. *Neurology* **80**, 2022–2027

55. Kenney, C., Powell, S., and Jankovic, J. (2007) Autopsy-proven Huntington's disease with 29 trinucleotide repeats. *Mov. Disord.* **22**, 127–130

56. Groen, J. L., de Bie, R. M. A., Foncke, E. M. J., Roos, R. A. C., Leenders, K. L., and Tijssen, M. A. J. (2010) Late-onset Huntington disease with intermediate CAG repeats: true or false? *J. Neurol. Neurosurg. Psychiatry* **81**, 228–230

57. Pieri, L., Madiona, K., Bousset, L., and Melki, R. (2012) Fibrillar α-synuclein and huntingtin exon 1 assemblies are toxic to the cells. *Biophys. J.* **102**, 2894–2905

58. Boeddrich, A., Gaumer, S., Haacke, A., Tzvetkov, N., Albrecht, M., Evert, B. O., Müller, E. C., Lurz, R., Breuer, P., Schugardt, N., Plassmann, S., Xu, K., Warrick, J. M., Suopanki, J., Wüllner, U., Frank, R., Hartl, U. F., Bonini, N. M., and Wanker, E. E. (2006) An arginine/lysine-rich motif is crucial for VCP/p97-mediated modulation of ataxin-3 fibrillogenesis. *EMBO J.* **25**, 1547–1558

59. Robertson, A. L., Headey, S. J., Saunders, H. M., Ecroyd, H., Scanlon, M. J., Carver, J. a, and Bottomley, S. P. (2010) Small heat-shock proteins interact with a flanking domain to suppress polyglutamine aggregation. *Proc. Natl. Acad. Sci. U. S. A.* **107**, 10424–10429

60. Tam, S., Spiess, C., Auyeung, W., Joachimiak, L., Chen, B., Poirier, M. A., and Frydman, J. (2009) The chaperonin TRiC blocks a huntingtin sequence element that promotes the conformational switch to aggregation. *Nat. Struct. Mol. Biol.* **16**, 1279–1285

61. Tam, S., Geller, R., Spiess, C., and Frydman, J. (2006) The chaperonin TRiC controls polyglutamine aggregation and toxicity through subunit-specific interactions. *Nat. Cell Biol.* **8**, 1155–1162

62. Baldo, B., Weiss, A., Parker, C. N., Bibel, M., Paganetti, P., and Kaupmann, K. (2012) A Screen for Enhancers of Clearance Identifies Huntingtin as a Heat Shock Protein 90 (Hsp90) Client Protein. *J. Biol. Chem.* **287**, 1406–1414

63. Redeker, V., Bonnefoy, J., Le Caer, J.-P., Pemberton, S., Laprévote, O., and Melki, R. (2010) A region within the C-terminal domain of Ure2p is shown to interact with the molecular chaperone Ssa1p by the use of cross-linkers and mass spectrometry. *FEBS J.* **277**, 5112–5123

64. Månsson, C., Kakkar, V., Monsellier, E., Sourigues, Y., Härmark, J., Kampinga, H. H., Melki, R., and Emanuelsson, C. (2013) DNAJB6 is a peptide-binding chaperone which can suppress amyloid fibrillation of polyglutamine peptides at substoichiometric molar ratios. *Cell Stress Chaperones* **19**, 227–239

65. Gu, X., Greiner, E. R., Mishra, R., Kodali, R., Osmand, A., Finkbeiner, S., Steffan, J. S., Thompson, L. M., Wetzel, R., and Yang, X. W. (2009) Serines 13 and 16 Are Critical Determinants of Full-Length Human Mutant Huntingtin Induced Disease Pathogenesis in HD Mice. *Neuron* **64**, 828–840

66. Robertson, A. L., Horne, J., Ellisdon, A. M., Thomas, B., Scanlon, M. J., and Bottomley, S. P. (2008) The structural impact of a polyglutamine tract is location-dependent. *Biophys. J.* **95**, 5922–5930

67. Darnell, G., Orgel, J. P. R. O., Pahl, R., and Meredith, S. C. (2007) Flanking polyproline sequences inhibit beta-sheet structure in polyglutamine segments by inducing PPII-like helix structure. *J. Mol. Biol.* **374**, 688–704

68. Ellisdon, A. M., Thomas, B., and Bottomley, S. P. (2006) The two-stage pathway of ataxin-3 fibrillogenesis involves a polyglutamine-independent step. *J. Biol. Chem.* **281**, 16888–16896

69. Fiumara, F., Fioriti, L., Kandel, E. R., and Hendrickson, W. A. (2010) Essential role of coiled coils for aggregation and activity of Q/N-rich prions and PolyQ proteins. *Cell* **143**, 1121–1135

70. O'Shea, E. K., Klemm, J. D., Kim, P. S., and Alber, T. (1991) X-ray structure of the GCN4 leucine zipper, a two-stranded, parallel coiled coil. *Science* **254**, 539–544

FIGURE LEGENDS

Figure 1. Aggregation of HttEx1Qn of pathological and non-pathological lengths. (**A**) Schematic representation of the primary structure of the different HttEx1Qn-derived polypeptides used in this study. (**B**,**C**) Monitoring of HttEx1Qn assembly; examples of HttEx1Q25 (B) and HttEx1Q48 (C) (20 μM each). For each reaction, aliquots were withdrawn at different time intervals and loaded on a tris-glycine SDS-PAGE gel. The gel was then stained with SYPRO Orange and the bands corresponding to soluble and insoluble HttEx1Qn quantified. (**D**) Assembly kinetics of HttEx1Q48 obtained by measuring i-thioflavin T binding (triangles), ii-the disappearance of SDS-soluble species (solid circles) or iii-the formation of SDS-insoluble aggregates (open circles) on SDS-PAGE. In each case, assembly is expressed as a fraction of the maximum signal. Each data point corresponds to the mean and associated standard error calculated from 3 to 10 independent experiments. (**E**) Time course of aggregation for HttEx1Qn (20 μM) of different polyQ stretch lengths at 37°C. Each data point corresponds to the mean and associated standard error calculated from 3 to 10 independent experiments. (**F**) Half-time ($t_{1/2}$) of HttEx1Qn aggregation is correlated to the polyQ stretch length. Each data point corresponds to the mean and associated standard error calculated from 3 to 10 independent experiments. Solid line represents the best linear fit; the r^2 and p values of the linear regression are indicated. (**G**) Nature of species present at steady state for HttEx1Q17 (left panel) and HttEx1Q48 (right panel), assessed by negative stained electron microscopy and filter-trapping in triplicates (insets). (**H**) SDS-resistance of HttEx1Qn fibrils. Top panel, SDS-resistant material present at the end of the aggregation process of HttEx1Qn of different polyQ lengths trapped in the wells of an SDS-PAGE. The gel was stained by SYPRO Orange (Invitrogen) and the signal quantified using the software Multigauge (Life Science Systems). The relative means and associated standard errors calculated from three independent experiments are represented in the bottom panel.

Figure 2. Assembly of HttEx1Q48 in the presence of Hsc70. (**A,B**) Activity of Hsc70. (A) Luciferase assay. Refolding of chemically denatured luciferase (0.1 μM) in the absence (open circles) or in the presence of Hsc70 (20 μM; solid circles). Each data point corresponds to the mean and associated standard error calculated from 3 independent experiments. (B) [γ^{32}P]ATP hydrolysis. ATPase activity of Hsc70 alone (20 μM; open circles) or in the presence of luciferase (0.1 μM; solid circles) or HttEx1Q48 (20 μM; open crosses). We measured Hsc70 ATPase activity after extraction of the [^{32}P] phosphomolybdate complex formed in 1 N HCl, at 30°C in assembly buffer. Each data point corresponds to the mean and associated standard error calculated from 3 independent experiments. (**C,D**) Representative examples of HttEx1Q48 assembly (20 μM) in the presence of 5 μM (C) or 20 μM (D) Hsc70. For each reaction, aliquots were withdrawn at different time intervals and loaded on a tris-glycine SDS-PAGE gel. The gel was then stained with SYPRO Orange and the bands corresponding to soluble and insoluble HttEx1Q48 quantified. (**E,F**) Effect of Hsc70 on HttEx1Q48 kinetics of assembly. (E), Time courses of HttEx1Q48 (20 μM) assembly at 37°C with increasing concentrations of Hsc70 (0-40 μM), in the absence (dashed lines) or the presence (solid lines) of 1 mM ATP. Each data point corresponds to the mean and associated standard error calculated from 3 to 10 independent experiments. (F), Half maximal effective Hsc70 concentration. The inverse of assembly half-time ($1/t_{1/2}$) for HttEx1Q48 at a constant concentration (20 μM) was determined for increasing Hsc70 concentrations (0-40 μM). Each data point corresponds to the mean and associated standard error calculated from 3 to 10 independent experiments. (**G,H**) Hsc70 does not bind to HttEx1Qn fibrils. Hsc70 (20 μM) was incubated alone or in the presence of HttEx1Q48 fibrils (20 μM monomer concentration) for 1h at 37°C. The reaction was done in triplicate. The reaction mixtures were centrifuged for 20 min at 16000g, and the corresponding pellets and supernatants were loaded on SDS-PAGE (G). The gel was then stained with SYPRO Orange, the bands corresponding to Hsc70 in the pellet and the supernatant were quantified and the calculated mean and standard error values are represented (H). Statistical significance corresponds to t-tests.

Figure 3. Assembly of HttEx1Q48 in the presence of the cochaperones Hdj1 and Hdj2. (**A,B**) Activity of the cochaperones. (A) Luciferase assay. Refolding of chemically denatured luciferase (0.1 μM) in the absence (open circles) or in the presence of Hdj1 or Hdj2 (20 μM each; solid circles). Each data point corresponds to the mean and associated standard error calculated from 3 independent experiments. (B) [γ^{32}P]ATP hydrolysis. ATPase activity of Hdj1 and Hsc70 (green; 10 μM each) or Hdj2 and Hsc70 (blue; 10 μM each) in the presence of luciferase (0.1 μM; solid circles) or HttEx1Q48 (20 μM; open crosses). Each data point corresponds to the mean and associated standard error calculated from 3 independent experiments. (**C,D**) Representative examples of HttEx1Q48 assembly (20 μM) in the presence of Hdj2 (2.5 μM) and in the absence (C) or the presence (D) of Hsc70 (2.5 μM). For each reaction, aliquots were withdrawn at different time intervals and loaded on a tris-glycine SDS-PAGE gel. The gel was then stained with SYPRO Orange and the bands corresponding to soluble and insoluble HttEx1Q48 quantified. (**G**), Time courses of HttEx1Q48 (20 μM) assembly at 37°C in the absence or presence of Hsc70 and/or Hdj1 or Hdj2 (2.5 μM each). Each data point corresponds to the mean and associated standard error calculated from 3 independent experiments. (**H**), Effect of the presence of both Hsc70 (2.5 μM) and one co-chaperone (Hdj1 or Hdj2; 2.5 μM each) on HttEx1Q48 assembly half-time at 20 μM. Black, calculated theoretical additive effects of the individual chaperones; grey, experimental measurements. Each data point corresponds to the mean and associated standard error calculated from 3 independent experiments. Statistical significance corresponds to t-tests; ***, $p<0.001$.

Figure 4. Structure-function relationship for HttEx1Q48 fibrils assembled in the absence or the presence of Hsc70. (**A**) Negative stained electron micrographs of HttEx1Q48 (20 μM) assembled in the presence of Hsc70 at equimolar concentration. (**B**) FTIR spectra of fibrillar HttEx1Q25 (green), HttEx1Q48 (red) and HttEx1Q48 assembled in the presence of equimolar concentrations of Hsc70 (HttEx1Q48$_{Hsc70}$; orange). As the same small quantity of Hsc70 was found in the pellet when the chaperone was incubated alone or in the presence of aggregating HttEx1Q48, HttEx1Q48$_{Hsc70}$ spectra is shown without the contribution of Hsc70; the latter is shown in black. Each data point corresponds to the mean calculated from 3 independent experiments; for the sake of clarity standard errors are shown every 5 cm^{-1}. The secondary structure contents are given in Table 1. (**C**) Nucleation propensities of HttEx1Q48 and HttEx1Q48$_{Hsc70}$ fibrils. The % of U2OS cells expressing stably the reporter protein HttEx1Q25-ChFP, with at least one focal HttEx1Q25-ChFP after treatment with exogenous HttEx1Q48 and HttEx1Q48$_{Hsc70}$ fibrils, 0.5 μM (monomers concentration), is indicated. Each data point corresponds to the mean and associated standard error calculated from 4 independent experiments. Statistical significance corresponds to t-tests; ***, $p<0.001$. Representative fluorescence micrographs of U2OS cells stably expressing the reporter protein HttEx1Q25-ChFP exposed or not to HttEx1Q48 and HttEx1Q48$_{Hsc70}$ fibrils are shown. Scale bar, 20 μm.

Figure 5. Hsc70 affects the assembly of HttEx1Qn of pathological and non-pathological lengths to a similar extent. Left panel: Time courses of HttEx1Qn (20 μM) assembly at 37°C with increasing concentrations of Hsc70 (0-40 μM). Right panel: Half maximal effective Hsc70 concentrations. The inverse of assembly half-times ($1/t_{1/2}$) for HttEx1Qn at a constant concentration (20 μM) were determined for increasing Hsc70 concentrations (0-40 μM). (A,F) HttEx1Q41; (B,G) HttEx1Q35; (C,H) HttEx1Q30; (D,I) HttEx1Q25; (E,J) HttEx1Q17. Each data point corresponds to the mean and associated standard error calculated from 3 to 6 independent experiments.

Figure 6. Hsc70 interacts with the 17 N-terminal amino acid residues of HttEx1Qn. (**A-B**) Hsc70 has no effect on HttEx1Qn-ΔNt$_{17}$ and Qn assembly. Time courses of (A) HttEx1Q35-ΔNt$_{17}$ and (B) Q35 (20 μM each) assembly at 37°C with increasing concentrations of Hsc70 (0-20 μM). Each data point corresponds to the mean and associated standard error calculated from 3 independent experiments. (**C,D**) Antagonistic effects of Hsc70 and free Nt$_{17}$ on HttEx1Q48 assembly. (C) Time course of HttEx1Q48 (20 μM) assembly at 37°C in the absence or presence of Hsc70 with or without Nt$_{17}$ at the indicated

concentrations. (D) Effect of the presence of both Hsc70 and Nt_{17} at the indicated concentrations on HttEx1Q48 (20 μM) assembly half-times ($\Delta t_{1/2}$). Black, theoretical additive effects of the individual polypeptides; grey, experimental measurements. Each data point corresponds to the mean and associated standard error calculated from 3 independent experiments. Statistical significances correspond to t-tests: ***, $p<0.001$; **, $p<0.01$. (**E**) Binding of dansyl-Nt_{17} (1 μM; solid columns) to increasing concentrations of Hsc70, HttEx1Q35, Q35 or HttEx1Q35-ΔNt_{17}, alone or in combination. As controls we also tested the binding of a scrambled version of dansyl-Nt_{17} (1 μM; dashed columns) and of free dansyl (1 μM; empty column). Each data point corresponds to the mean and associated standard error calculated from 3 to 6 independent experiments.

Figure 7. Identification of HttEx1Q25-Hsc70 interaction sites. (**A**) Coomassie blue stained 2D gel of the reaction products generated upon Hsc70 and HttEx1Q25 cross-linking using BS3-d0/d4. (**B**) Location of the Hsc70 lysine residues cross-linked to HttEx1Q25. The cross-linked peptides are given in Table 2. Lysine residues are depicted as orange sticks and cross-linked lysines are colored in red and shown as atom spheres. For each lysine from Hsc70 cross-linked to HttEx1Q25, the cross-linked threonine, lysine or N-terminal glycine residue from HttEx1Q25 is indicated. The Hsc70 3D model was built as described in Redeker *et al* (29). This figure was generated using PYMOL (http://www.pymol.org).

(**C-E**) Identification of the cross-link between peptide 494-500 from Hsc70 and peptide 1-8 from HttEx1Q25. (C) Mass spectrum of the triple charged cross-linked peptide with monoisotopic m/z 579.6293 and 580.9713 for the BS3-d0 and BS3-d4 peptides respectively. (D) Fragmentation spectrum of the precursor ion at m/z 580.97 corresponding to the first isotope of the BS3-d4 peptide. The identified fragments and their charge state are annotated. The star labels (*) indicate the fragments with the BS3-d4 cross-linker. (E) The identified fragments are indicated on the cross-linked sequences. The α and β sequences correspond to the 494-500 Hsc70 and the 1-8 HttEx1Q25 peptides, respectively. This cross-link involves residues K497 and the N-terminal G1 from Hsc70 and HttEx1Q25, respectively.

(**F-H**) Identification of the cross-link between peptide 551-561 from Hsc70 and 9-17 from HttEx1Q25. (F) Mass spectrum of the triple charged cross-linked peptide with monoisotopic m/z 813.1016 and 814.4431 for the BS3-d0 and BS3-d4 peptides, respectively. (G) Fragmentation spectrum of the precursor ion at m/z 813.4362 corresponding to the second isotope of the BS3-d0 peptide. The identified fragments are annotated, together with their charge state. The star labels (*) indicate the fragments with the BS3-d0 cross-linker. (H) The identified fragments are indicated on the cross-linked sequences. The α and β sequences correspond to the 551-561 Hsc70 and 9-17 HttEx1Q25 peptides, respectively. This cross-link involves residues K557 and K11 from Hsc70 and HttEx1Q25, respectively.

Figure 8. Role of the N-terminal flank in HttEx1Qn aggregation. (**A**) Mass spectrum of the double charged Ex1Q25-Ex1Q25 cross-linked peptide with monoisotopic m/z 905.4527 and 907.4648 for the BS3-d0 and BS3-d4 peptides respectively. (**B**) LTQ-Orbitrap fragmentation mass spectra of the first isotope of the BS3-d0 peptide at m/z 905.45 (upper spectrum) and the first isotope of the BS3-d4 peptide at m/z 907.46 (bottom spectrum). The identified fragments and their charge state are indicated. The star labels (*) indicate the fragments with the BS3-d0 or d4 cross-linker. The full circles indicate internal N-terminal fragments confirming the identified sequence, and the empty circles indicate fragment ions resulting from loss of water. As both α and β sequences correspond to the same 1-8 HttEx1Q25 sequence and generate identical α and β ion fragments masses, the α and β label of the ion fragment annotation has been suppressed. (**C**) The identified fragments are indicated on the HttEx1Q25 cross-linked sequences. The α and β sequences correspond to the two 1-8 HttEx1Q25 peptides respectively. This cross-link involves the N-terminal G1 residue from two HttEx1Q25 molecules. (**D**) Time courses of HttEx1Q35, HttEx1Q35-ΔNt_{17} and Q35 (20 μM each) assembly at 37°C. (**E-G**) Time course of HttEx1Q35 (E), HttEx1Q35-ΔNt_{17} (F) and Q35 (G) (20 μM each) assembly at 37°C with increasing concentrations of free Nt_{17}. For all the kinetics (panels D-G), each data point corresponds to the mean and associated standard error calculated from 3 to 6 independent experiments.

Figure 9. Model for HttEx1Qn aggregation and the effect of Hsc70. (**A**) CD spectra of free Nt_{17}. The circular dichroism spectrum of the free Nt_{17} peptide (2 mM) shows that it assembles into coil coil quaternary structure ($\Theta_{222}/\Theta_{208}$= 1.16). (**B**) The coiled-coil model for HttEx1Qn was built using the structure of GCN4 leucine zipper coiled-coil (PDB 2ZTA (70)). Nt_{17} sequence was aligned onto GCN4 sequence to identify the leucine residues involved in the coiled-coil interaction. (**C**) The two-steps aggregation model of HttEx1Qn. HttEx1Qn coalescence is driven by homotypic interactions between the N-terminal flanks. PolyQ-polyQ interactions stabilize the nuclei and certainly contribute to fibrils elongation at a later stage. (**D**) Mode of action of Hsc70. Hsc70 interferes with the aggregation process by interacting with the N-terminal flank, competing against the homotypic Nt_{17}-Nt_{17} interactions and thus impeding the initial coalescence between HttEx1Qn molecules. The resulting fibrils differ in terms of structural and infectious properties.

Table 1. Secondary structure content of different types of HttEx1Qn fibrils estimated from FTIR spectroscopy measurements.

Secondary structure	HttEx1Q25 fibrils	HttEx1Q48 fibrils	HttEx1Q48 fibrils formed in the presence of Hsc70
lateral chains	9 %	13 %	13 %
amyloid	28 %	43 %	30 %
β-sheets (non amyloid)	16 %	3 %	14 %
α-helices	13 %	12 %	12 %
others	34 %	31 %	29 %

Table 2. List of the identified Hsc70-HttEx1Q25 cross-linked peptides

BS3-d0 peptides			BS3-d4 peptides			Hsc70 peptides			HttEx1Q25 peptides			ΔM
M exp	z	*m/z*	M exp	z	*m/z*	segment	XL site	Sequence	segment	XL site	Sequence	(ppm)
1735.8644	3	579.63	1739.89043	3	580.97	494-500	K497	STG**k**ENK	1-8	G1	**g**AM[16]ATLEK	1.8
2132.0678	3	711.70	2136.09353	3	713.04	558-567	K561	LQG**k**INDEDK	1-8	G1	**g**AM[16]ATLEK	2.6
2190.1100	3	731.05	2194.13273	3	732.39	551-561	K557	ATVEDE**k**LQGK	1-8	G1	**g**AM[16]ATLEK	2.7
2388.2199	4	598.06	2388.2415	4	598.07	558-569	K561	LQG**k**INDEDKQK	1-8	G1, T5	**g**AM[16]A**t**LEK	1.7
2436.2813	3	813.10	2440.30583	3	814.44	551-561	K557	ATVEDE**k**LQGK	9-17	K11	LM[16]**k**AFESLK	1.7
2924.5319	3	975.85	2928.52043	3	977.18	452-469	K458	DNNLLGkFELTGIPPAPR	1-8	G1	**g**AM[16]ATLEK	1.7
3160.5823	4	791.15	3164.6023	4	792.16	551-569	K561	ATVEDEKLQG**k**INDEDKQK	1-8	G1	**g**AM[16]ATLEK	2

For each identified cross-linked peptide in the Hsc70-HttEx1Q25 complex, the table gives the experimental mass (M exp), the charge state (z), the *m/z* ratio for both the BS3G-d0 and the BS3-d4 cross-linked peptides, the amino acid segment, the cross-linked residues (XL site) and the amino acid sequence for both the Hsc70 and the HttEx1Q25 peptides. ΔM (ppm) corresponds to the mass deviation between the experimental mass and the theoretical mass of the identified BS3-d0 cross-linked peptides, given by the XBobCat software (http://prottools.ethz.ch/orinner/public/htdocs/xquest/xLynx_review.html) (33).

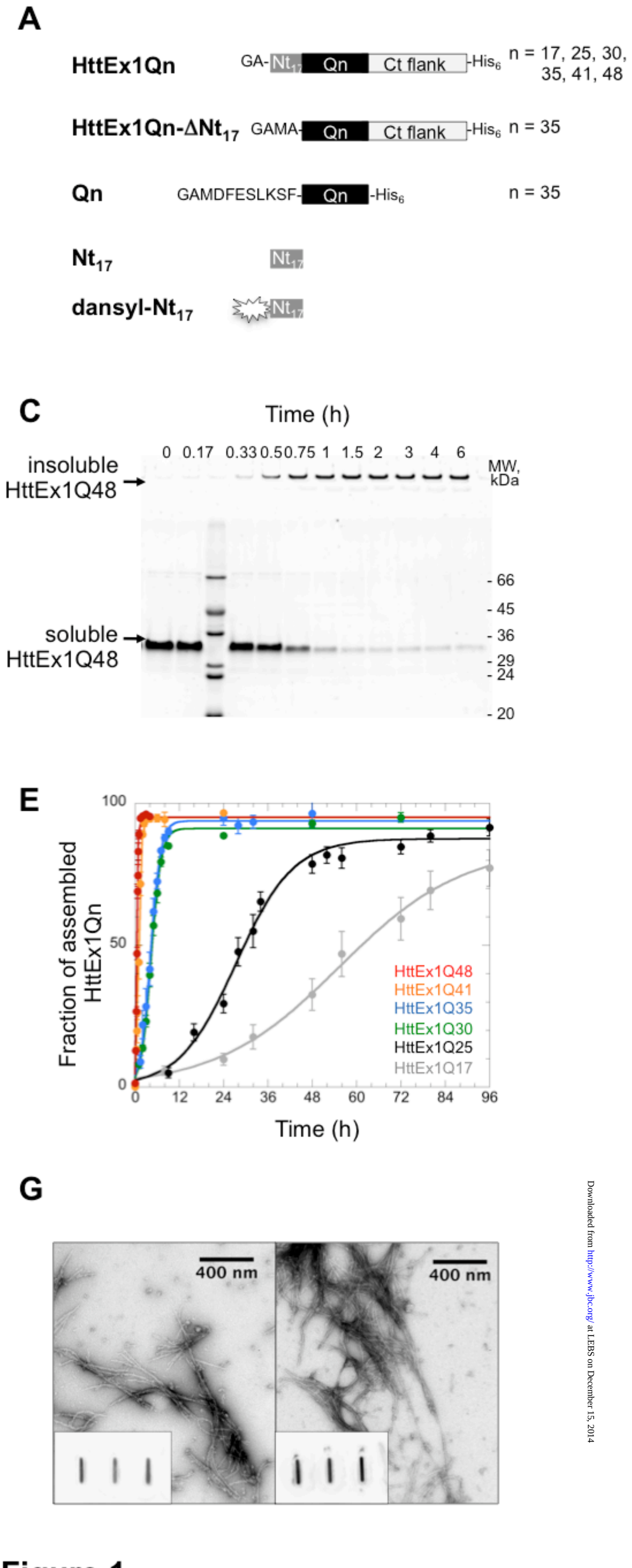

Figure 1

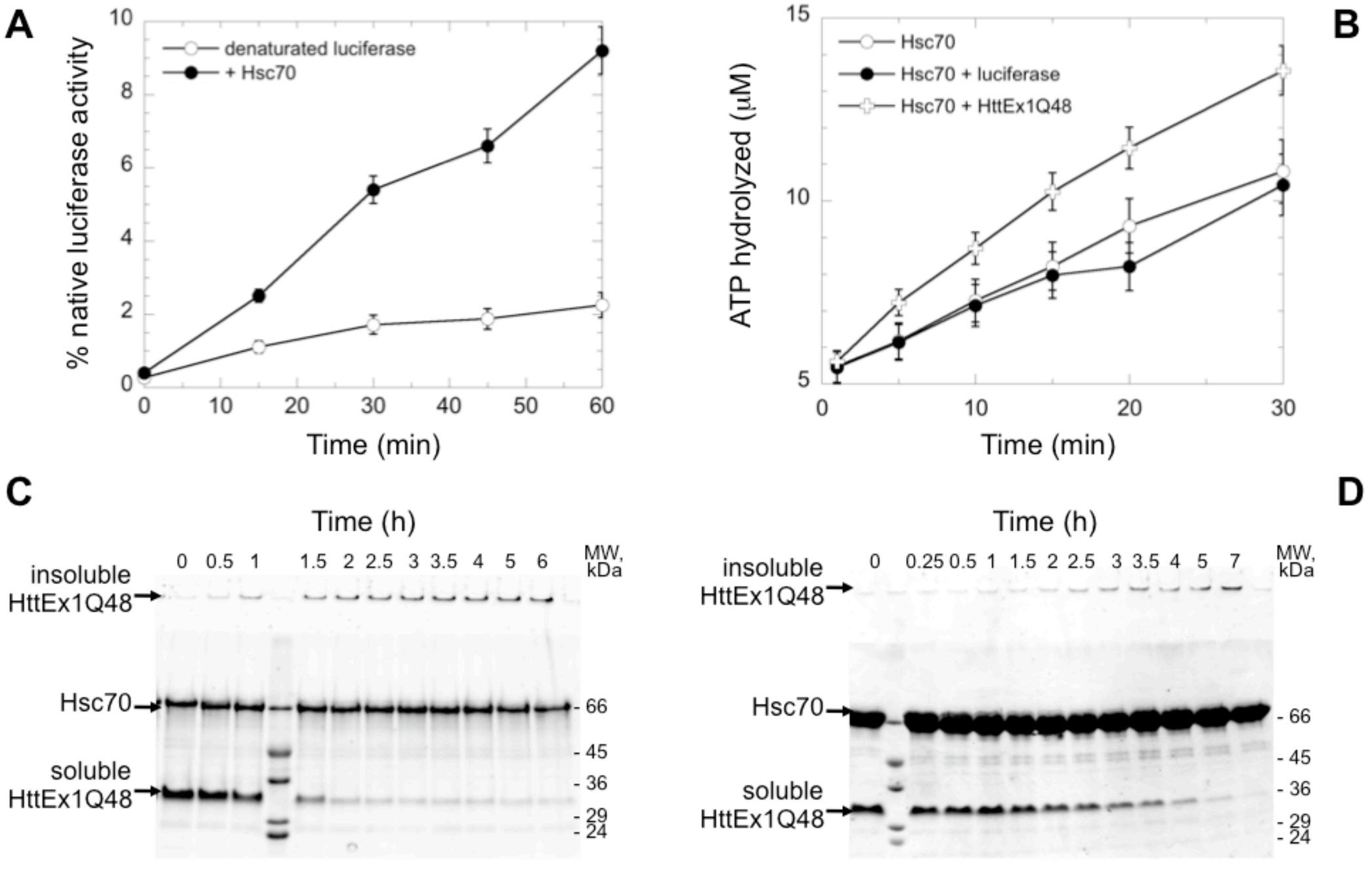

Figure 2

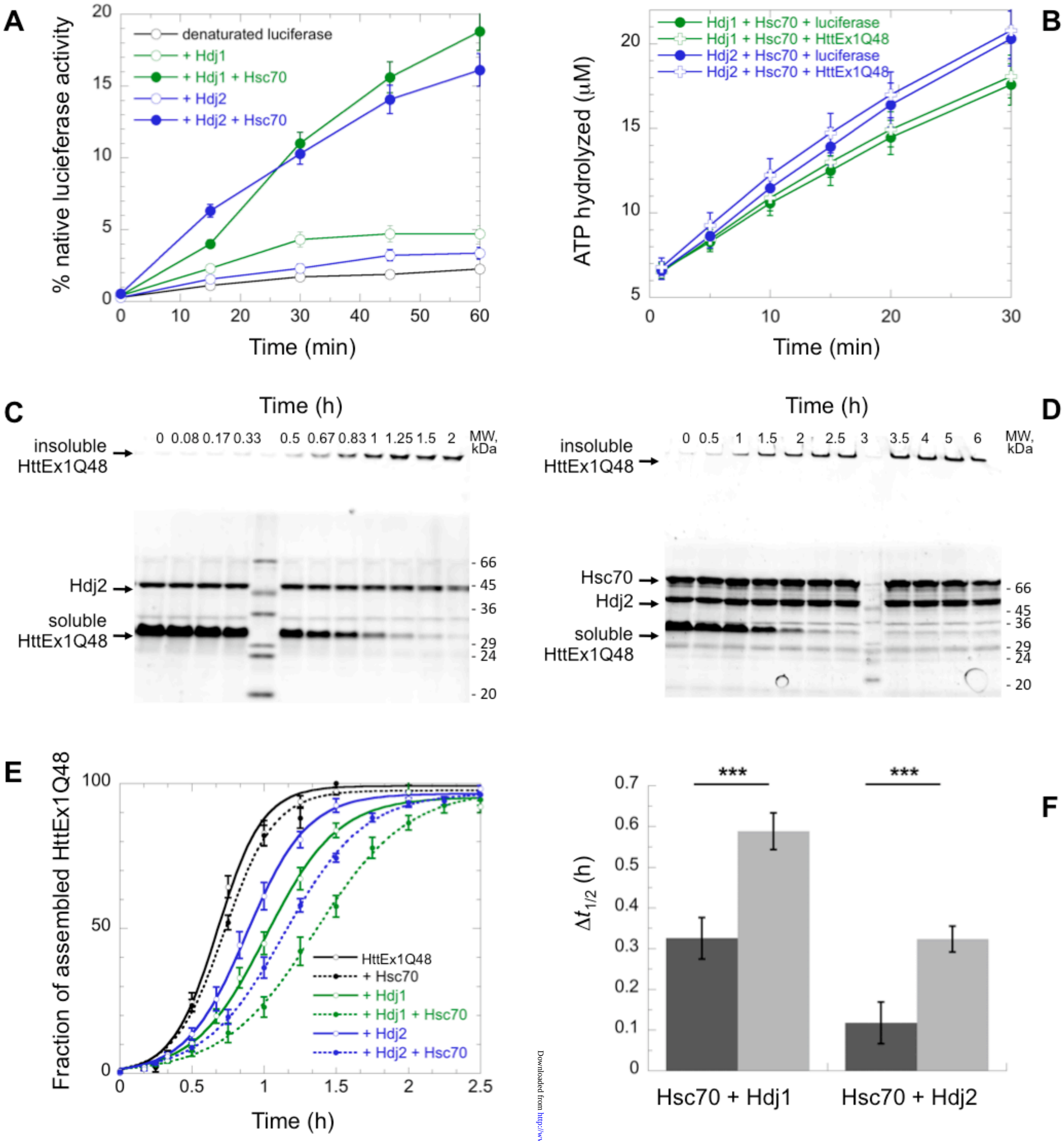

Figure 3

A

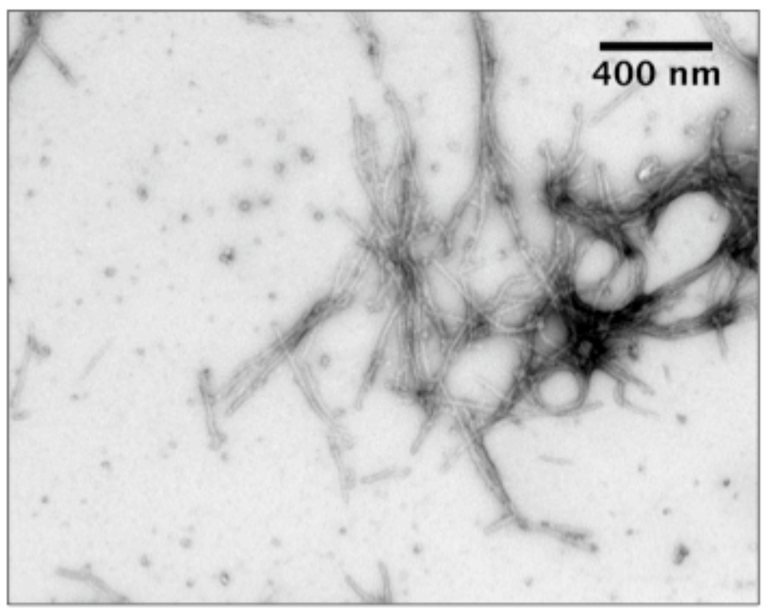

B

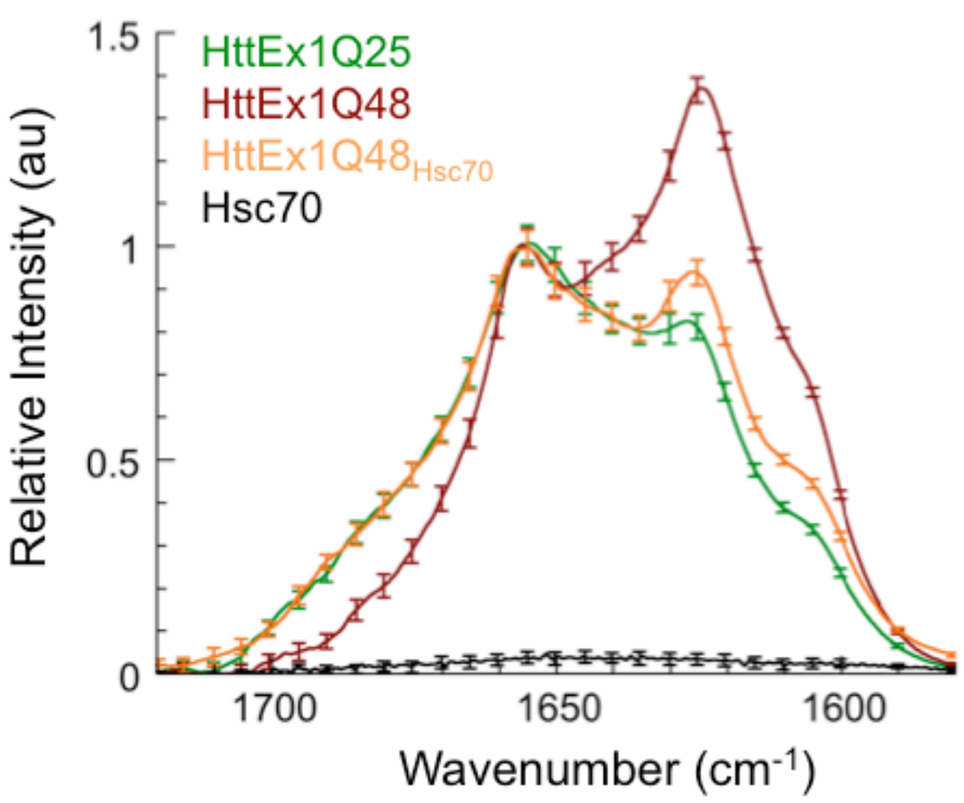

C

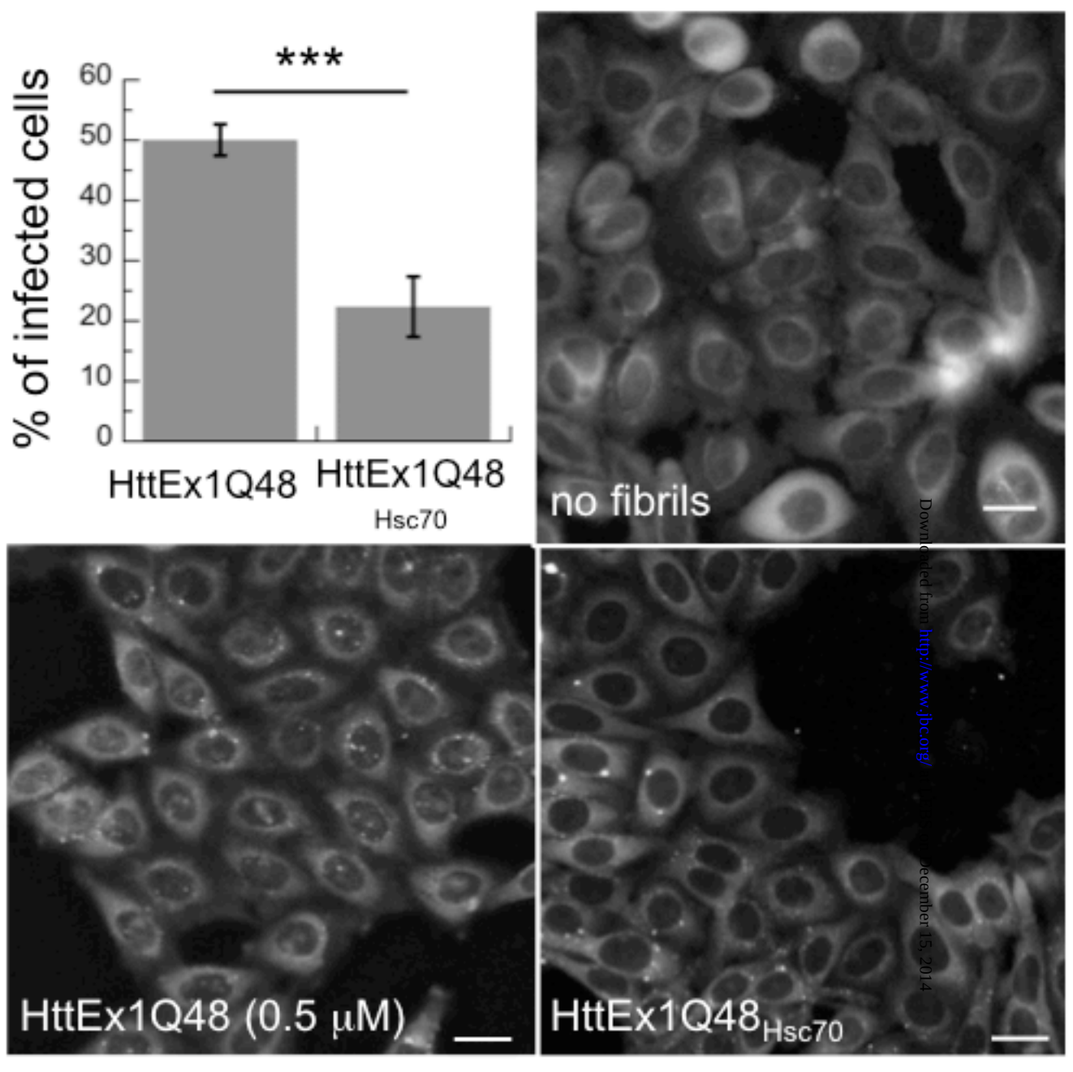

Figure 4

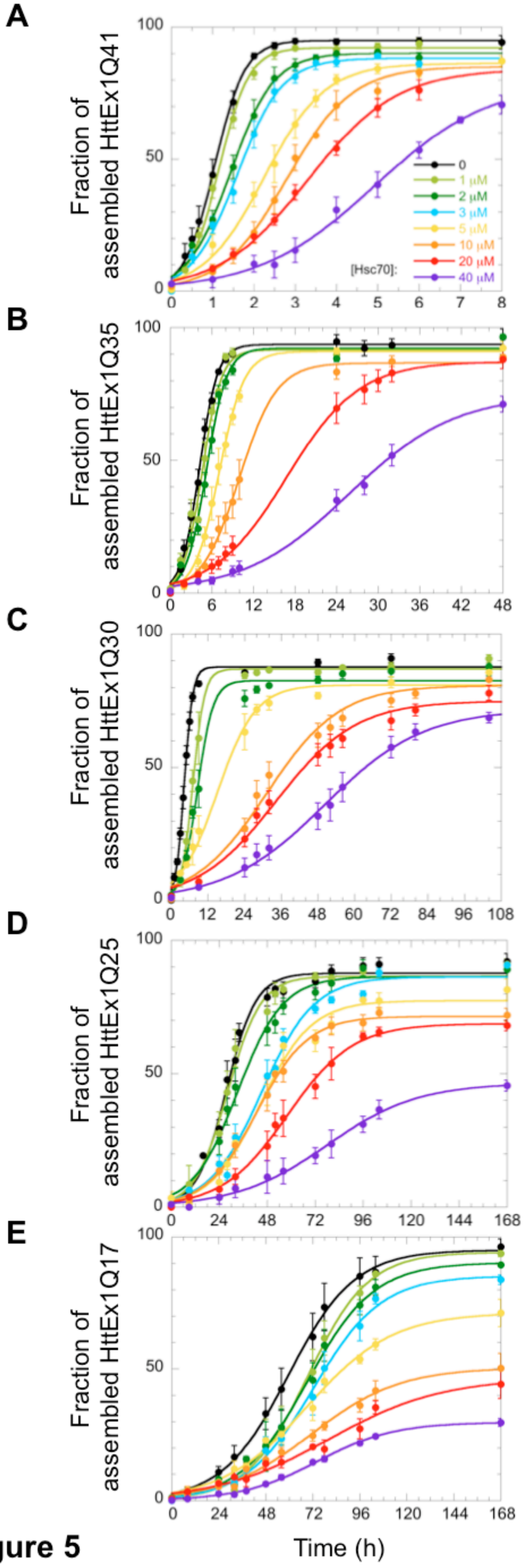

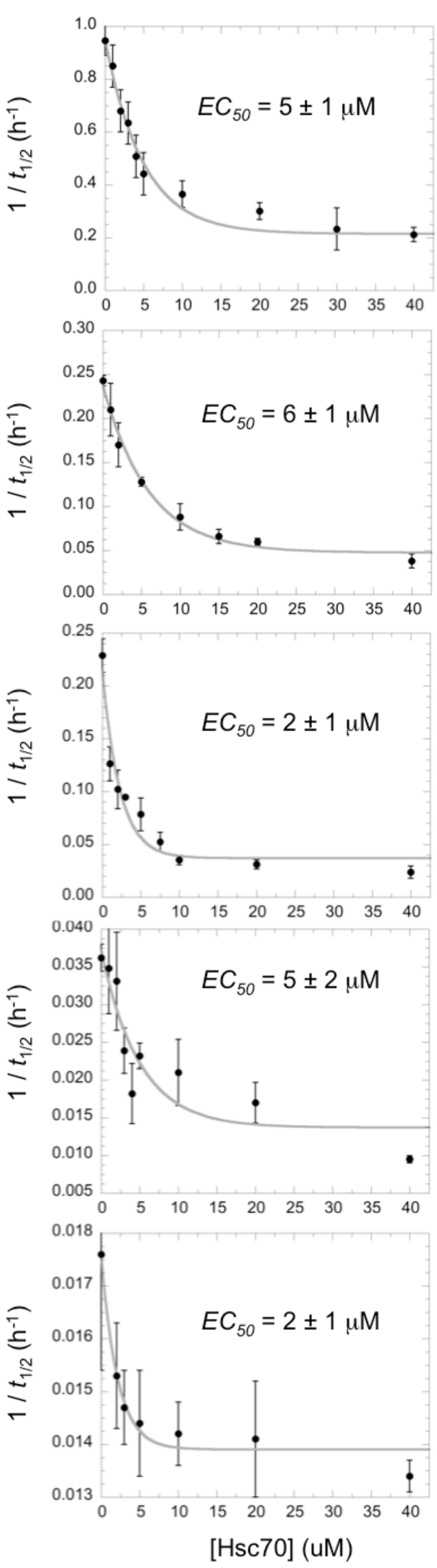

Figure 5

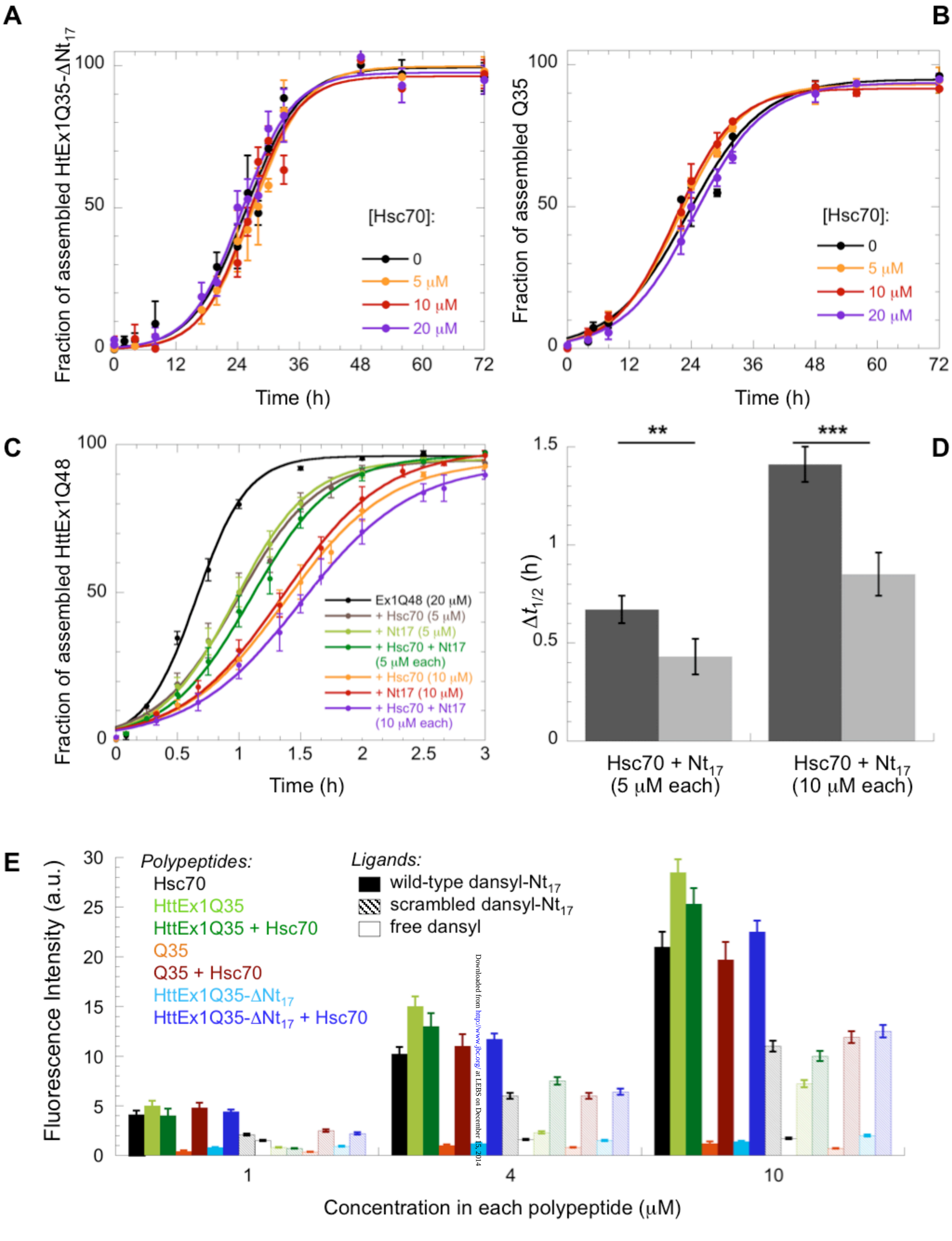

Figure 6

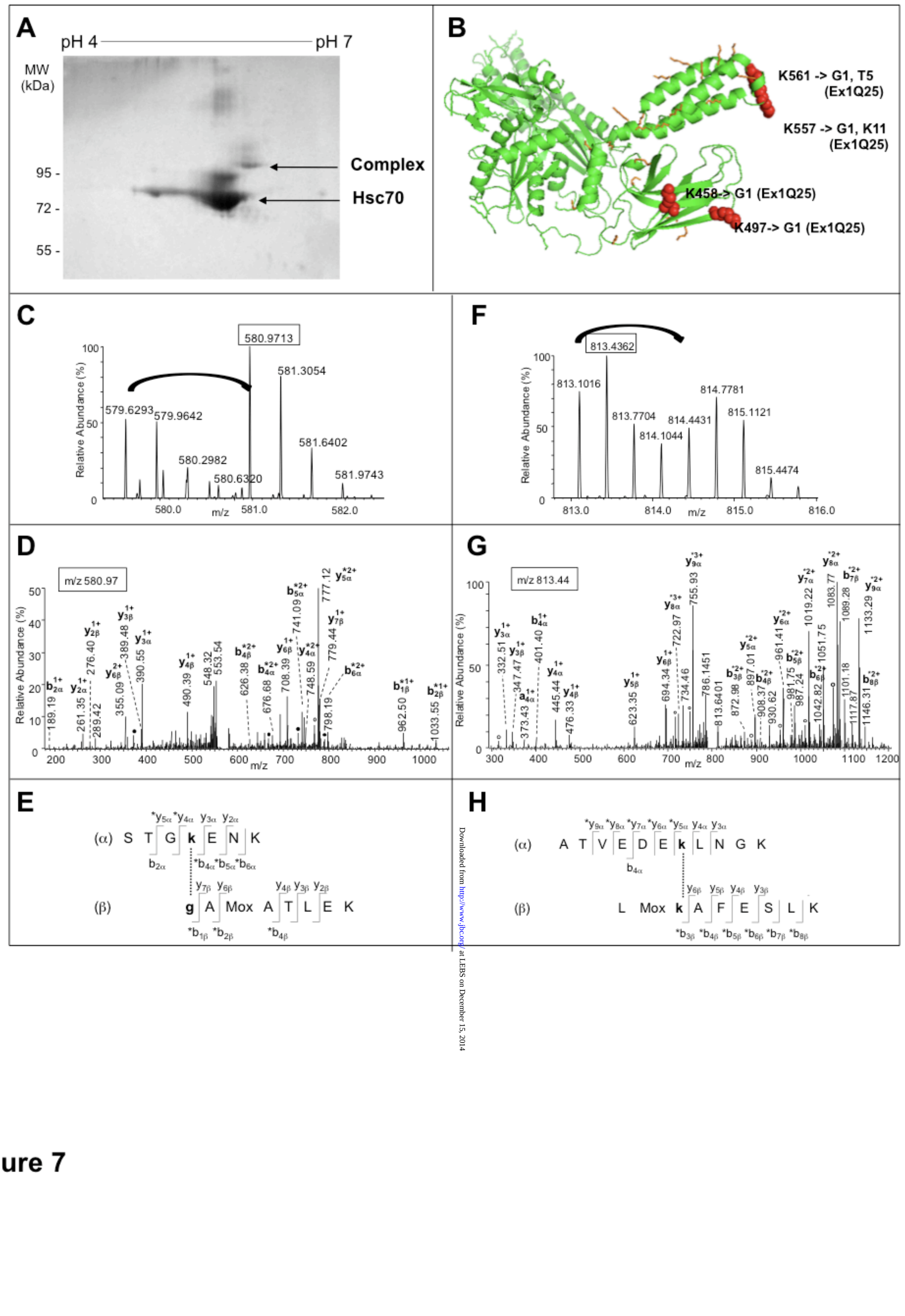

Figure 7

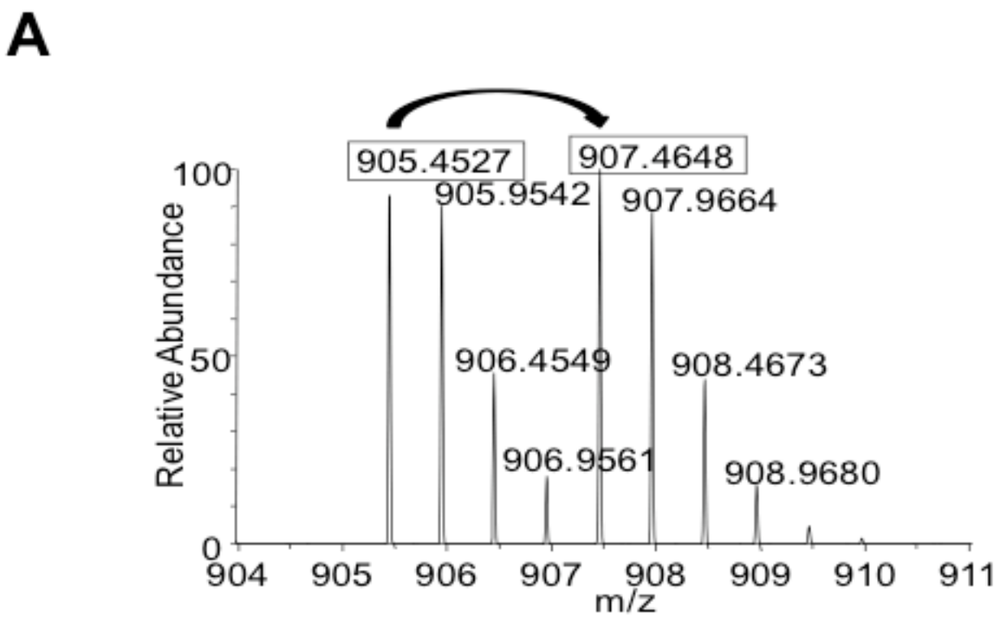

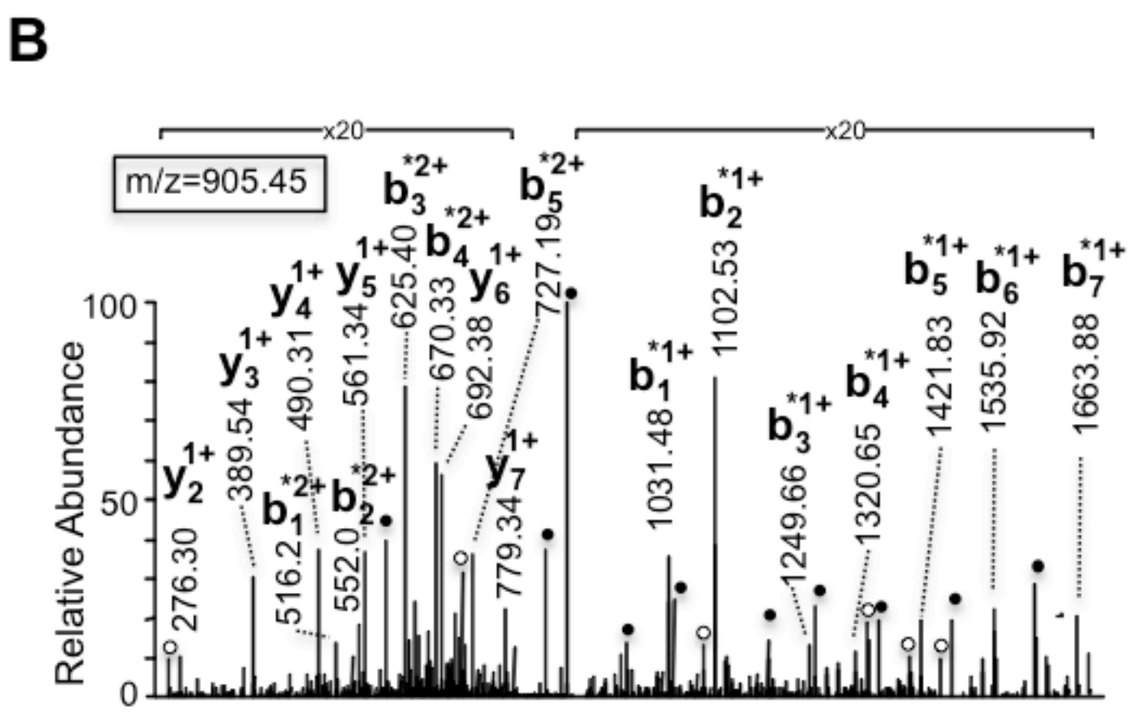

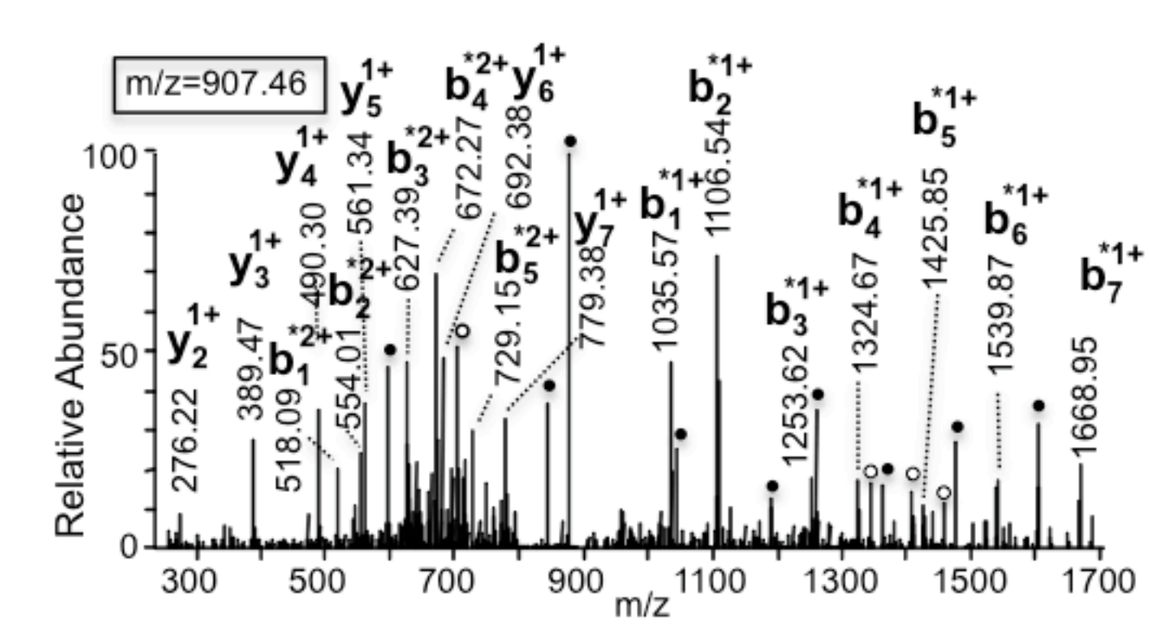

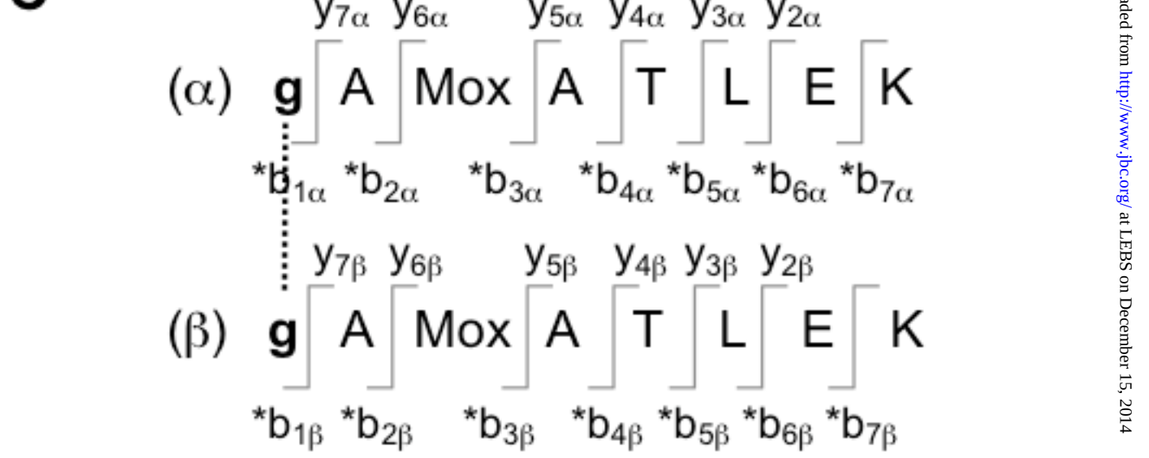

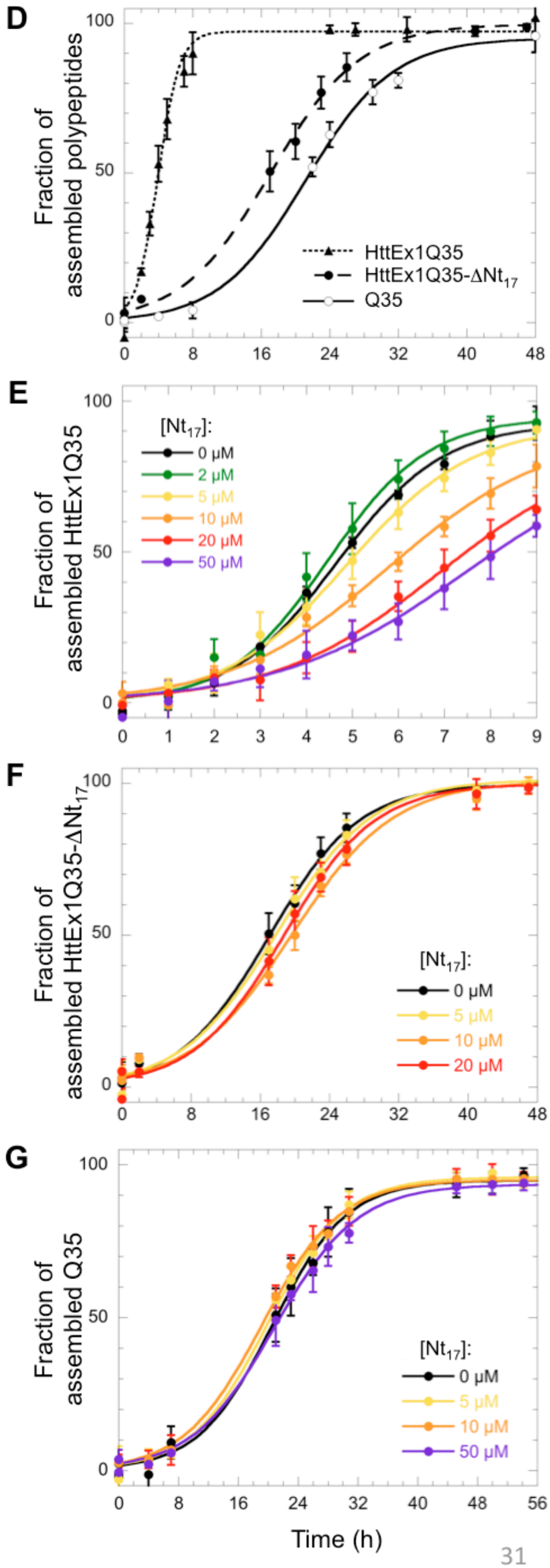

Figure 8

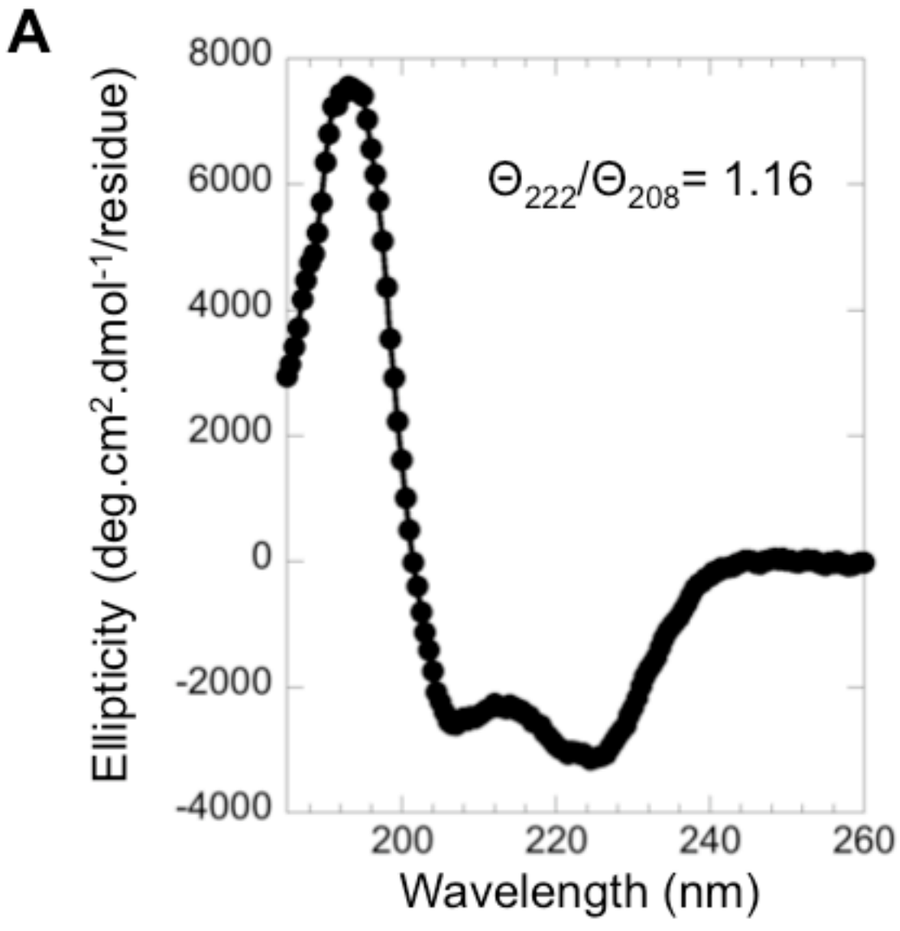

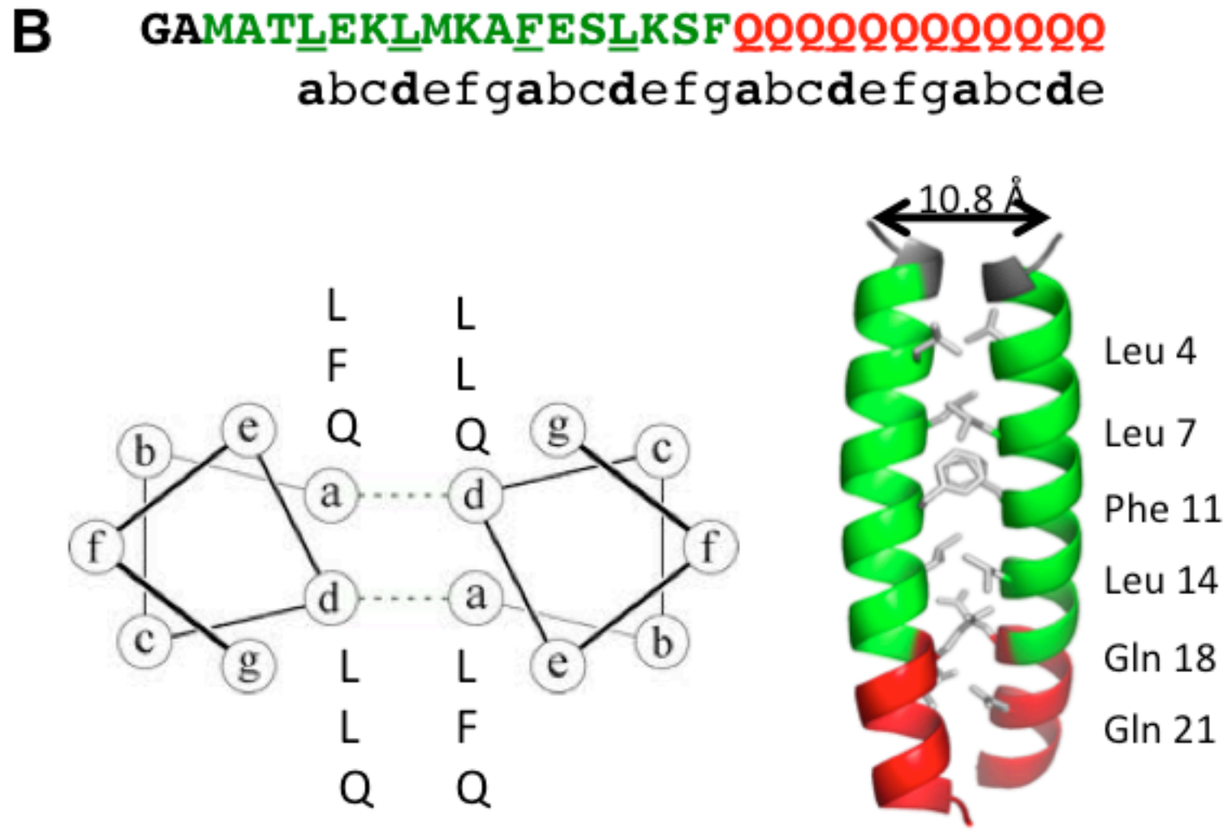

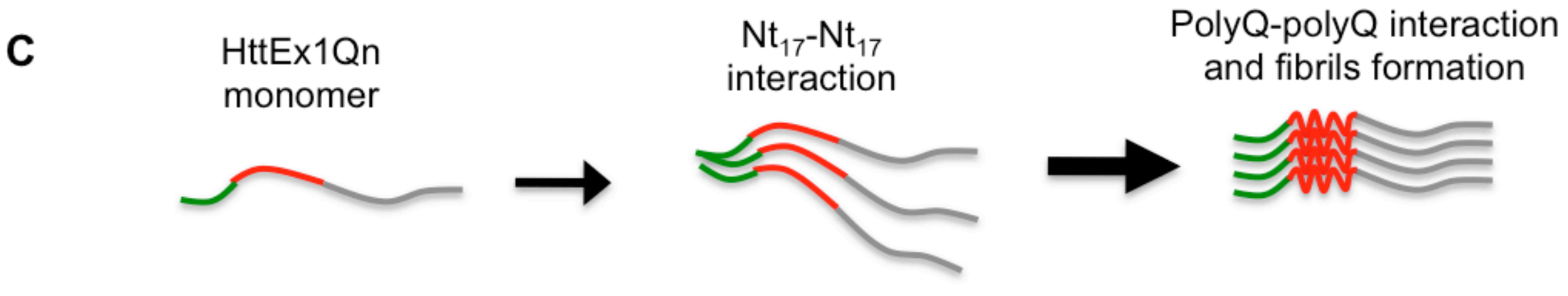

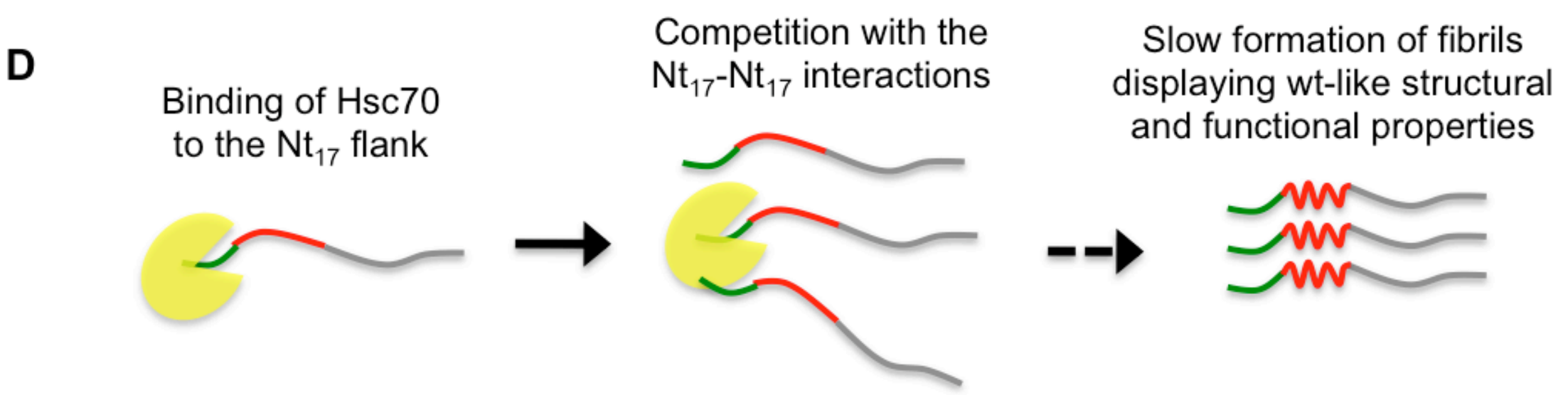

Figure 9